J|A|C|S
ARTICLES
Published on Web 06/28/2006

Scope and Mechanism of the C−H Bond Activation Reactivity within a Supramolecular Host by an Iridium Guest: A Stepwise Ion Pair Guest Dissociation Mechanism

Dennis H. Leung, Robert G. Bergman,* and Kenneth N. Raymond*

Contribution from the Department of Chemistry, University of California, Berkeley, California 94720-1460

Received February 28, 2006; E-mail: rbergman@berkeley.edu; raymond@socrates.berkeley.edu

Abstract: A chiral self-assembled supramolecular M_4L_6 assembly has been shown to be a suitable host for a series of reactive monocationic half-sandwich iridium guests **1**, **3**, and **4** that are capable of activating C−H bonds. Upon encapsulation, selective C−H bond activation of organic substrates occurs. Precise size and shape selectivity are observed in the C−H bond activation of aldehydes and ether substrates. The reactions exhibit significant kinetic diastereoselectivities. Thermodynamic studies have shown that the iridium starting materials and products are bound strongly by the host assembly. The encapsulation process is largely entropy-driven. Kinetic investigations with water-soluble phosphine traps and added salts have provided evidence for a unique stepwise mechanism of guest dissociation for [**4** ⊂ Ga_4L_6]. Iridium guest **4** first dissociates from the host cavity to form an ion pair with the host exterior. This species then fully dissociates from the host exterior into the bulk solution. Model ion pair intermediates were characterized directly with ^{1}H NMR NOESY techniques. The rate of iridium guest dissociation is slower than the rate observed for the C−H bond activation processes, indicating that the selective C−H bond activation reactivity occurs within the cavity of the supramolecular host.

Introduction

In recent years, supramolecular host−guest chemistry has emerged as an important way to study how encapsulating molecules into well-defined spatial environments can mediate their chemical reactivity.[1,2] Lehn, Cram, and Pedersen introduced crown ethers and cryptands as simple host molecules.[3,4] Naturally occurring cyclodextrins have also been shown to be effective host molecules for controlling reactivity.[5−11] As target guest molecules have grown larger and more complex, self-assembly has been harnessed to design supramolecular hosts capable of encapsulating larger reactive species as guests within well-defined cavities. Much like enzymes, the size, shape, and chemical environment of a supramolecular assembly cavity can help control the recognition and reactivity of substrate molecules, offering the potential for new types of synthetic catalysts.

Raymond and co-workers have demonstrated an efficient approach to the self-assembly of highly symmetric metal−ligand supramolecular structures which display unique properties.[12−16] The most robust of these assemblies forms an $[M_4L_6]^{12-}$ [M = Ga(III), Al(III), Fe(III)] cluster, in which six bis-catecholamide naphthalene-based ligands (L^{4-}) coordinate to four trivalent metal centers (M^{3+}) along the edges of a tetrahedron (Figure 1).[12] The highly negatively charged assembly is only soluble in polar solvents such as water and methanol but contains a hydrophobic internal cavity of ∼300−500 Å^3. Although the individual metal and ligand components are achiral, the overall assemblies are homochiral due to the rigid mechanical coupling of the ligand, which results in exclusively ΔΔΔΔ or ΛΛΛΛ configuration with respect to the coordination at the four metal vertices. While the host assembly can be resolved to obtain each enantiomer,[17,18] the racemic structure was used in these studies.

The M_4L_6 assembly has been shown to selectively encapsulate a variety of water-soluble monocationic guests such as alkylammonium cations[12,19−21] and organometallic species[22−26] within its cavity to form host−guest assemblies of the general formula

(1) Lehn, J.-M. *Supramolecular Chemistry: Concepts and Perspectives*; VCH: Weinheim, 1995.
(2) Steed, J. W.; Atwood, J. L. *Supramolecular Chemistry*; John Wiley & Sons: Ltd: Chichester, 2000.
(3) Lehn, J.-M. *Angew. Chem., Int. Ed. Engl.* **1988**, *27*, 89−112.
(4) Cram, D. J. *Angew. Chem., Int. Ed. Engl.* **1988**, *27*, 1009−1020.
(5) Breslow, R.; Guo, T. *J. Am. Chem. Soc.* **1988**, *110*, 5613−5617.
(6) Breslow, R.; Anslyn, E. *J. Am. Chem. Soc.* **1989**, *111*, 8931−8932.
(7) Breslow, R.; Schmuck, C. *J. Am. Chem. Soc.* **1996**, *118*, 6601−6606.
(8) Breslow, R.; Zhang, X.; Xu, R.; Maletic, M. *J. Am. Chem. Soc.* **1996**, *118*, 11678−11679.
(9) Breslow, R.; Huang, Y.; Zhang, X.; Yang, J. *Proc. Natl. Acad. Sci. U.S.A.* **1997**, *94*, 11156−11158.
(10) Breslow, R.; Dong, S. D. *Chem. Rev.* **1998**, *98*, 1997−2012.
(11) Takahashi, K. *Chem. Rev.* **1998**, *98*, 2013−2034.
(12) Caulder, D. L.; Powers, R. E.; Parac, T. N.; Raymond, K. N. *Angew. Chem., Int. Ed.* **1998**, *37*, 1840−1843.
(13) Caulder, D. L.; Raymond, K. N. *J. Chem. Soc., Dalton Trans.* **1999**, 1185−1200.
(14) Caulder, D. L.; Raymond, K. N. *Acc. Chem. Res.* **1999**, *32*, 975−982.
(15) Caulder, D. L.; Bruckner, C.; Powers, R. E.; Konig, S.; Parac, T. N.; Leary, J. A.; Raymond, K. N. *J. Am. Chem. Soc.* **2001**, *123*, 8893−8938.
(16) Yeh, R. M.; Xu, J.; Seeber, G.; Raymond, K. N. *Inorg. Chem.* **2005**, *44*, 6228−6239.
(17) Terpin, A. J.; Ziegler, M.; Johnson, D. W.; Raymond, K. N. *Angew. Chem., Int. Ed.* **2001**, *40*, 157−160.
(18) Ziegler, M.; Davis, A. V.; Johnson, D. W.; Raymond, K. N. *Angew. Chem., Int. Ed.* **2003**, *42*, 665−668.

10.1021/ja061412w CCC: $33.50

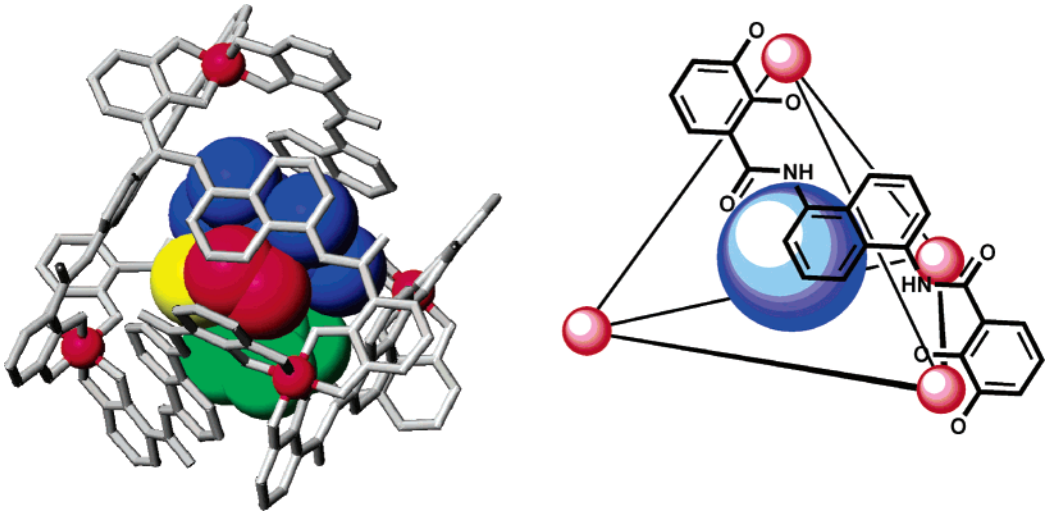

Figure 1. (Left) CAChe[41] MM3 optimized model of $[Cp^*(PMe_3)Ir(Me)(C_2H_4) \subset Ga_4L_6]^{11-}$. (Right) Schematic of $[G \subset M_4L_6]^{11-}$. Six bis-bidentate catechol amide ligands span the edges of the tetrahedron (only one of the ligands is drawn for clarity).

$[G \subset M_4L_6]^{11-}$ ($\subset$ denotes guest encapsulation within the host). Encapsulation is highly dependent on the charge, size, shape, and hydrophobicity of the entering guest species.[19] While these host−guest assemblies can be characterized by mass spectrometry, NMR spectroscopy is the most diagnostic technique to determine encapsulation. The NMR resonances for guests within the cavity are shifted upfield by 2−3 ppm due to the anisotropic ring current effect of the naphthalene walls of the host.[27] Recently, the guest exchange processes for this system have been studied.[28,29] The ability of the host assembly to exchange guest molecules suggested that substrate access into the host cavity could occur readily, resulting in the formation of a synthetic active site.

This host−guest behavior raised the possibility of mediating organometallic reactivity through supramolecular encapsulation.[30] Selective encapsulation of organometallic catalysts provides a method of preparing synthetic mimics of metalloenzyme active sites, and some success in this area has been reported.[31−40] Rather than using covalently bound ligands to induce changes in reactivity, the supramolecular environment of a host cavity may be used to obtain selective reactivity. In particular, self-assembly provides a route to easily prepare large, complex chiral cavities that may mediate asymmetric reactivity without the need for costly step-by-step chiral ligand synthesis.

We have previously reported that the $Na_{12}[Ga_4L_6]$ host is capable of encapsulating the cationic half-sandwich iridium species $Cp^*(PMe_3)Ir(Me)(C_2H_4)^+$ (**1**) (Figure 1).[23] Complex **1** is a cationic analogue of the neutral complex $Cp^*(PMe_3)Ir(Me)(OTf)$, which has been shown to be highly active in the C−H bond activation of organic substrates.[42−44] In the absence of the host, **1** is chemically reactive and, at elevated temperatures (~75 °C over several days), is able to activate the C−H bonds of aldehyde substrates, resulting in the formation of a new monocationic iridium alkyl carbonyl species **2-R** (Scheme 1).[44,45]

Upon heating $[\mathbf{1} \subset Ga_4L_6]$ at similar temperatures, the resulting host−guest assembly displays highly specific size and shape substrate selectivities not exhibited in the absence of the host. For example, sterically demanding aldehyde substrates such as pivaldehyde or benzaldehyde are too large to enter the cavity of the host and, thus, cannot react with the iridium metal center. In addition to size, shape also plays an important role in substrate selectivity: 2-methyl-butyraldehyde is not activated by the host−guest assembly, but addition of iso-steric 3-methyl-butyraldehyde results in substrate activation. Due to the chirality of the $Na_{12}[Ga_4L_6]$ host and the chiral-at-metal iridium products, the resulting host−guest assemblies are formed with varying degrees of diastereoselectivity, depending on the size and shape of the product formed.

(19) Parac, T. N.; Caulder, D. L.; Raymond, K. N. *J. Am. Chem. Soc.* **1998**, *120*, 8003−8004.
(20) Fiedler, D.; Bergman, R. G.; Raymond, K. N. *Angew. Chem., Int. Ed.* **2004**, *43*, 6748−6751.
(21) Fiedler, D.; Leung, D. H.; Bergman, R. G.; Raymond, K. N. *Acc. Chem. Res.* **2005**, *38*, 351−360.
(22) Fiedler, D.; Pagliero, D.; Brumaghim, J. L.; Bergman, R. G.; Raymond, K. N. *Inorg. Chem.* **2004**, *43*, 846−848.
(23) Leung, D. H.; Fiedler, D.; Bergman, R. G.; Raymond, K. N. *Angew. Chem., Int. Ed.* **2004**, *43*, 963−966.
(24) Fiedler, D.; Leung, D. H.; Bergman, R. G.; Raymond, K. N. *J. Am. Chem. Soc.* **2004**, *126*, 3674−3675.
(25) Tiedemann, B. E. F.; Raymond, K. N. *Angew. Chem., Int. Ed.* **2006**, *45*, 83−86.
(26) Fiedler, D.; Bergman, R. G.; Raymond, K. N. *Angew. Chem., Int. Ed.* **2006**, *45*, 745−748.
(27) Sutherland, I. O. *Chem. Soc. Rev.* **1986**, *15*, 63−91.
(28) Davis, A. V.; Raymond, K. N. *J. Am. Chem. Soc.* **2005**, *127*, 7912−7919.
(29) Davis, A. V.; Fiedler, D.; Seeber, G.; Zahl, A.; van Eldik, R.; Raymond, K. N. *J. Am. Chem. Soc.* **2006**, *128*, 1324−1333.
(30) Davis, A. V.; Yeh, R. M.; Raymond, K. N. *Proc. Natl. Acad. Sci. U.S.A.* **2002**, *99*, 4793−4796.
(31) Ito, H.; Kusukawa, T.; Fujita, M. *Chem. Lett.* **2000**, *29*, 598−599.
(32) Slagt, V. F.; Reek, J. N. H.; Kramer, P. C. J.; van Leeuwen, P. W. N. M. *Angew. Chem., Int. Ed.* **2001**, *40*, 4271−4274.
(33) Slagt, V. F.; van Leeuwen, P. W. N. M.; Reek, J. N. H. *Angew. Chem., Int. Ed.* **2003**, *42*, 5619−5623.
(34) Slagt, V. F.; Kramer, P. C. J.; van Leeuwen, P. W. N. M.; Reek, J. N. H. *J. Am. Chem. Soc.* **2004**, *126*, 1526−1536.
(35) Merlau, M. L.; Mejia, M. d. P.; Nguyen, S. T.; Hupp, J. T. *Angew. Chem., Int. Ed.* **2001**, *40*, 4239−4242.
(36) Morris, G. A.; Nguyen, S. T.; Hupp, J. T. *J. Mol. Catal. A* **2001**, *174*, 15−20.
(37) Lee, S. J.; Hu, A.; W., L. *J. Am. Chem. Soc.* **2002**, *124*, 12948−12949.
(38) Jiang, H.; Hu, A.; Lin, W. *Chem. Commun.* **2003**, 96−97.
(39) Gianneschi, N. C.; Bertin, P. A.; Nguyen, S. T.; Mirkin, C. A.; Zakharov, L. N.; Rheingold, A. L. *J. Am. Chem. Soc.* **2003**, *125*, 10508−10509.
(40) Gianneschi, N. C.; Cho, S.-H.; Nguyen, S. T.; Mirkin, C. A. *Angew. Chem., Int. Ed.* **2004**, *43*, 5503−5507.
(41) *CAChe*, 5.04 ed.; Fujitsu Limited, 2002.
(42) Burger, P.; Bergman, R. G. *J. Am. Chem. Soc.* **1993**, *115*, 10462−10463.
(43) Arndsten, B. A.; Bergman, R. G. *Science* **1995**, *270*, 1970−1973.
(44) Klei, S. R.; Golden, J. T.; Burger, P.; Bergman, R. G. *J. Mol. Catal. A.* **2002**, *189*, 79−94.
(45) Alaimo, P. J.; Arndsten, B. A.; Bergman, R. G. *Organometallics* **2000**, *2000*, 2130−2143.

Scheme 1

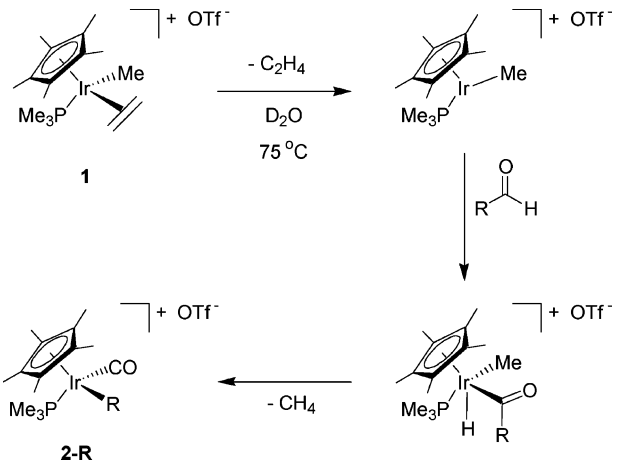

Encapsulation of More Reactive Iridium Guests

While these initial results were promising, wider substrate scope and milder reaction conditions were desired. At 75 °C, decomposition and precipitation of the host−guest assembly occur, which results in only a moderate yield of 40−60% for the overall reaction. In addition, the activation of more demanding organic substrates such as alkanes and arenes was not observed with **1**, as temperatures greater than 75 °C resulted in decomposition of **1**. The low relative reactivity of **1** is due to the strongly bound ethene ligand that must first dissociate to form the reactive 16 e^- metal species (Scheme 1). Therefore, one key to increasing the reactivity of the iridium guest is to make the coordinating ligand more labile. As a result, we chose to examine how changing the substitution on the ethene ligand would affect its lability and the resulting reactivity of the iridium complex.

The analogous iridium olefin compounds are easily prepared by layering an atmosphere of the alkene gas over a solution of the neutral $Cp^*(PMe_3)Ir(Me)(OTf)$ complex dissolved in CH_2Cl_2. The displacement of OTf^- to form the cationic alkene species $[Cp^*(PMe_3)Ir(Me)(olefin)][OTf]$ is immediate and results in a color change from deep orange to pale yellow (eq 1). $Cp^*(PMe_3)Ir(Me)(propene)^+$ (**3**) and $Cp^*(PMe_3)Ir(Me)(cis$-2-butene$)^+$ (**4**) were prepared using this method. Due to the enantiotopic faces of the coordinating propene ligand, **3** is formed as a mixture of four diastereomers (two of which are enantiomers) with a diastereomeric ratio (dr) of 74:26.

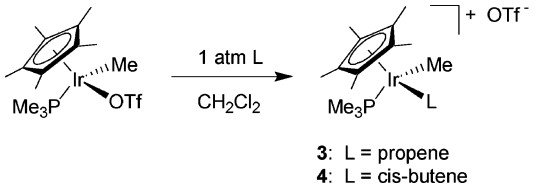

(1)

The incorporation of methyl substituents on the coordinated alkene results in much higher activity for the iridium species. The propene complex **3** is capable of activating aldehyde substrates at 45 °C over a period of several days. Even more strikingly, the *cis*-butene complex **4** activates aldehyde substrates at room temperature in quantitative yield after 30 min.

Both **3** and **4** proved to be suitable guests for encapsulation within the $Na_{12}[Ga_4L_6]$ supramolecular host. Since the iridium guests are chiral-at-metal, two diastereomeric host−guest assemblies are formed. The encapsulation of the initial iridium ethene guest **1** has a low level of recognition with a dr of 55:45. However, [**3** ⊂ Ga_4L_6] and [**4** ⊂ Ga_4L_6] exhibited higher levels of diastereoselectivity; the methyl substituents change the effective size and shape of the encapsulated iridium guest. Encapsulation of the two diastereomers of **3** by $Na_{12}[Ga_4L_6]$ results in the possible formation of a racemic mixture of eight diastereomeric host−guest complexes (four of which are enantiomers). However, only three pairs of diastereomers of [**3** ⊂ Ga_4L_6] are observed with a dr of 50:40:10. The *cis*-butene complex **4** is encapsulated by the $Na_{12}[Ga_4L_6]$ host with a dr of 70:30 (Figure 2).

Addition of appropriately sized aldehyde substrates to [**4** ⊂ Ga_4L_6] led to formation of the corresponding encapsulated iridium carbonyl products [**2-R** ⊂ Ga_4L_6] as was observed before. Due to the mild conditions required with **4**, near quantitative yields of the host−guest product were obtained at room temperature in 30 min. There is little qualitative change in the rate of reaction upon encapsulation. Presumably, appropriately sized substrates are able to readily access the host cavity, and the initial dissociation of *cis*-butene remains rate limiting in both the free and encapsulated cases. Moreover, the same steric substrate selectivities were observed with this system as with [**1** ⊂ Ga_4L_6] (Table 1).[46]

However, due to the milder reaction conditions, some aldehyde substrates [**4** ⊂ Ga_4L_6] afforded kinetic diastereoselective product formation. This is best illustrated in the C−H bond activation of propionaldehyde with [**4** ⊂ Ga_4L_6] (Table 1, entry 2). At room temperature after 30 min, complete formation of the encapsulated **2-Et** product is observed with a dr of 40:60, favoring the diastereomer opposite to that observed with [**1** ⊂ Ga_4L_6] at 75 °C. When this 40:60 mixture of diastereomers is heated to 75 °C for several hours, the dr equilibrates to the thermodynamic ratio 60:40 (Scheme 2). This implies that the host cavity selectively recognizes a kinetic diastereomeric state during the course of the iridium aldehyde activation rather than simply the product species, a key characteristic of many enzyme-catalyzed reactions.[47] The initial diastereomeric products that are formed are stable within the host cavity until heating allows for thermodynamic diastereoselective recognition of the products to occur.

Expanded Substrate Scope

In addition to providing a more efficient activation of aldehyde substrates, the high reactivity of **4** resulted in the extension of the substrate scope to other organic substrates. Analogous to the neutral $Cp^*(PMe_3)Ir(Me)(OTf)$ complex, **4** readily reacted with ethers,[44,48] dihydrogen,[44,49] and strained alkanes such as cyclopropane[42,44] under mild conditions. The corresponding encapsulated species [**4** ⊂ Ga_4L_6] displayed similar reactivity (Scheme 3).

In the absence of the host assembly, **4** proved capable of activating a variety of methyl alkyl ethers in aqueous solution

(46) Over the course of 24 h, [4 ⊂ Ga_4L_6] does react with benzaldehyde, presumably through dissociation from the host. This will be discussed in more detail below.
(47) Jencks, W. P. *Catalysis in Chemistry and Enzymology*; McGraw-Hill: New York, 1969.
(48) Luecke, H. F.; Arndsten, B. A.; Burger, P.; Bergman, R. G. *J. Am. Chem. Soc.* **1996**, *118*, 2517−2518.
(49) Golden, J. T.; Andersen, R. A.; Bergman, R. G. *J. Am. Chem. Soc.* **2001**, *123*, 5837−5838.

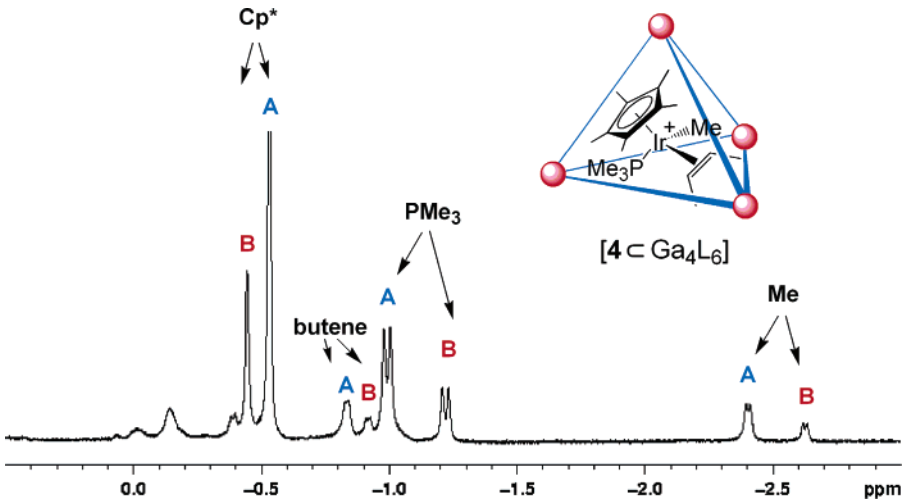

Figure 2. ^{1}H NMR spectrum of [**4** ⊂ Ga_4L_6] in D_2O displaying resonances shifted upfield. Considerable diastereoselective recognition is observed (A being the major diastereomer and B being the minor diastereomer).

Table 1. Diastereomeric Ratios Observed in the Reaction of [**4** ⊂ Ga_4L_6] with Aldehyde Substrates

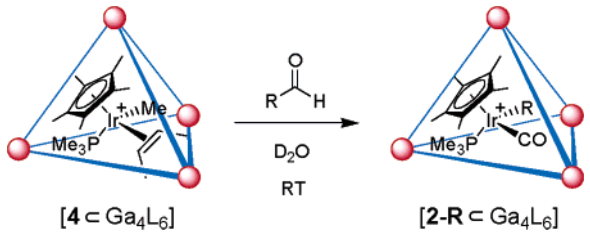

Entry	Substrate	dr	Entry	Substrate	dr
1		55 : 45	7	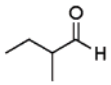	n. r.
2		40 : 60[a] 60 : 40	8	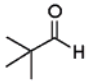	n. r.
3	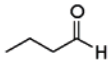	70 : 30	9		55 : 45
4	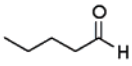	n. r.	10		n. r.
5		55 : 45	11	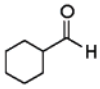	n. r.
6	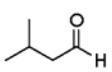	57 : 43	12	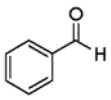	n. r.

[a] Kinetic diastereoelective product ratio of 40:60 observed. Heating products results in equilibration to a thermodynamic diastereomeric ratio of 60:40.

at a slightly elevated temperature of 45 °C over 1 h. These reactions occur by C−H bond activation of the methyl group α

Scheme 2

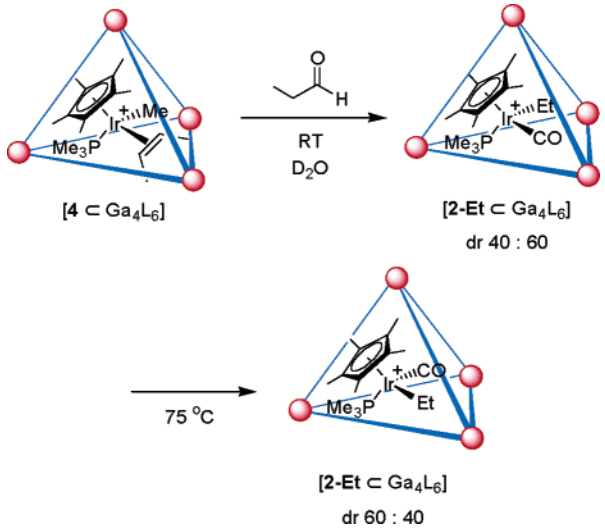

to the ethereal oxygen and loss of CH_4 followed by α-hydride elimination to form a Fischer carbene iridium product **5-R** (Scheme 4).[48]

When ethereal substrates were added to [**4** ⊂ Ga_4L_6] at 45 °C, the formation of the corresponding products [**5-R** ⊂ Ga_4L_6] was observed in good yield after 1 h. Similar to the reactions with aldehyde substrates, high substrate selectivity was observed (Table 2). In this case, only dimethyl ether and ethyl methyl ether were activated by the encapsulated iridium species (Table 2, entries 1 and 2). Methyl *n*-propyl ether and diethyl ether appear to be too long in the linear dimension to enter the host cavity. Due to the steric demands of the branched substituent, methyl isopropyl ether and methyl *tert*-butyl ether were also not activated. Cyclic ethers such as tetrahydrofuran were not activated. In contrast, in the absence of the supramolecular host, **4** reacts readily with all of these substrates.

Since the Fischer carbene iridium products **5-R** are chiral at the metal center, diastereomeric host−guest products were observed. In the case of the C−H bond activation of dimethyl ether, a large diastereomeric ratio of [**5-Me** ⊂ Ga_4L_6] was observed with a dr of 88:12 (Table 2, entry 1). Upon heating [**5-Me** ⊂ Ga_4L_6] to 75 °C for several hours, the host−guest diastereomers equilibrate to the thermodynamic diastereomeric

Scheme 3

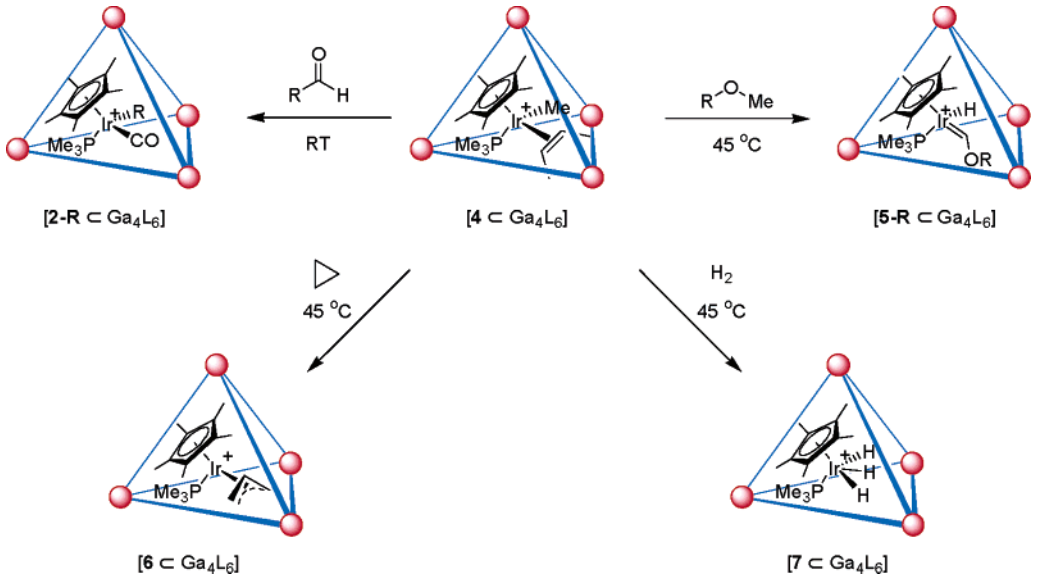

Scheme 4

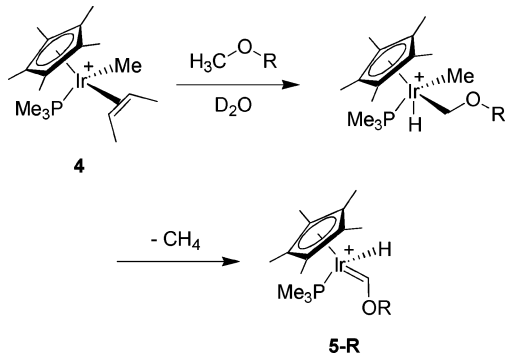

ratio 58:42 (Scheme 5). This is a further example of how the Ga_4L_6 supramolecular host displays high kinetic diastereoselectivity in the activation of organic substrates.

The encapsulated *cis*-butene complex [**4** ⊂ Ga_4L_6] was not active toward the C−H bond activation of many alkanes or arenes such as pentane and benzene even at elevated temperatures. It is possible that the low water solubility of these reactants precluded their use as efficient substrates for the host−guest assembly. Arene substrates are also sterically demanding and may not be able to enter the cavity. However, [**4** ⊂ Ga_4L_6] did react with the small hydrocarbon cyclopropane to form the achiral encapsulated π-allyl complex [**6** ⊂ Ga_4L_6] via ring opening[42,44] at 45 °C after 1 h in good yield (Scheme 3).

In addition, [**4** ⊂ Ga_4L_6] reacts with 1 atm of H_2 at 45 °C after 1 h to form the encapsulated iridium trihydride complex [**7** ⊂ Ga_4L_6] (Scheme 3).[44,49] One set of encapsulated guest resonances is observed in quantitative yield at room temperature. The iridium trihydride complex **7** has been shown to catalyze the H−D exchange of organic substrates in D_2O solvent.[50,51] However, addition of organic substrates such as aldehydes and ethers to [**7** ⊂ Ga_4L_6] resulted in no observable deuterium incorporation after extended periods of time at elevated temperatures.

(50) Skaddan, M. B.; Yung, C. M.; Bergman, R. G. *Org. Lett.* **2004**, *6*, 11−13.
(51) Yung, C. M.; Skaddan, M. B.; Bergman, R. G. *J. Am. Chem. Soc.* **2004**, *126*.

Table 2. Diastereomeric Ratios Observed in the Reaction of [**4** ⊂ Ga_4L_6] with Ethereal Substrates

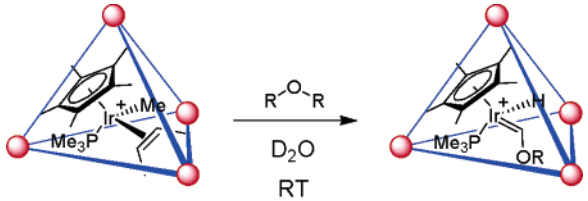

Entry	Substrate	dr	Entry	Substrate	dr
1		88 : 12[a] 58 : 42	5		n. r.
2		54 : 46	6	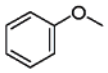	n. r.
3	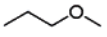	n. r.	7	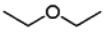	n. r.
4		n. r.	8		n. r.

[a] Kinetic diastereoselective product ratio of 88:12 observed. Heating results in equilibration to a thermodynamic dr of 58:42.

Thermodynamic Studies of Iridium Guest Binding

Having identified the encapsulation of several reactive iridium species, we sought to understand the mechanistic properties that govern the high substrate selectivities. Presumably, the highly selective activation reactions involving [**4** ⊂ Ga_4L_6] with organic substrates occur within the well-defined environment of the cavity. This may be particularly true for the activation of aldehydes, which occurs very cleanly under mild conditions. The fundamental stability of the host−guest assembly depends on the initial encapsulation of the reactive iridium species. To

Scheme 5

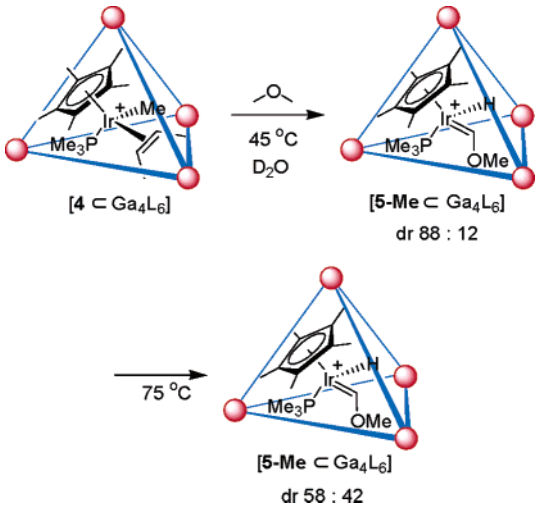

Table 3. Thermodynamic Binding Constants for the Encapsulation of Iridium Olefin Guests in D_2O (Includes Formation of Both Host−Guest Diastereomers)

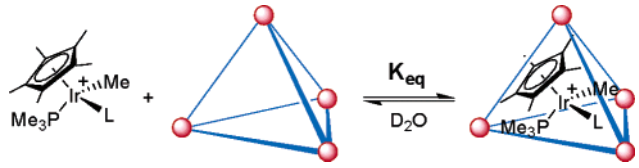

Guest	K_{eq} (M^{-1})	Guest	K_{eq} (M^{-1})
1	$2.5\ (3) \times 10^3$	4	$0.12\ (1) \times 10^3$
3	$0.7\ (7) \times 10^3$	6	$9.0\ (9) \times 10^3$

better understand the iridium encapsulation step, the thermodynamic binding constants (equilibrium constants for encapsulation) were measured for a variety of iridium starting materials and products. These binding constants were determined directly by ^{1}H NMR spectroscopy of a 10.0 mM solution of the host−guest assembly as well as by guest competition with tetraalkylammonium guests with known binding constants.[19] Encapsulation of the iridium species was expected to be facilitated by a combination of electrostatic attraction between the guest and the host as well as by π-cation interactions between the cationic guest and the aromatic walls of the host cavity.[52]

The iridium olefin guests are encapsulated effectively by the supramolecular host assembly, with binding constants on the order of $\sim 10^3$ M^{-1} (Table 3). The binding is strongest for the iridium ethene complex **1**. In contrast, placing methyl substituents on the alkene ligand may unfavorably increase the size of the guest and block potential π-stacking interactions between the guest and the naphthalene moiety on the host ligand scaffold, thereby reducing the favorable binding interactions for **3** and **4**. The comparatively high affinity of the iridium π-allyl complex **6**, compared to that of iridium propene guest **3**, may be due to a stronger interaction of its delocalized pi system with the naphthalene walls of the host cavity.

(52) Ma, J. C.; Dougherty, D. A. *Chem. Rev.* **1997**, *97*, 1303−1324.

Table 4. Themodynamic Binding Constants for the Encapsulation of Iridium Carbonyl Guests **2-R** in D_2O (Includes Formation of Both Host−Guest Diastereomers)

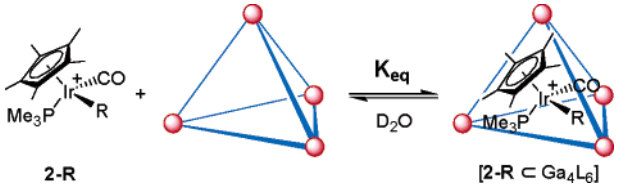

Guest	K_{eq} (M^{-1})	Guest	K_{eq} (M^{-1})
2-Me	$17\ (2) \times 10^3$	2-Pr	$5.9\ (6) \times 10^3$
2-Et	$15\ (2) \times 10^3$	2-^{i}Pr	$2.3\ (2) \times 10^3$

The binding is also sensitive to the size and shape of the iridium guest. This is most clearly seen with the encapsulation of the product iridium carbonyl species **2-R** (Table 4). The methyl carbonyl complex **2-Me** is bound strongly with a binding constant of $17(2) \times 10^3$ M^{-1}. However, as the size of the guest becomes too large, the binding affinity begins to decrease significantly. This is presumably due to the greater unfavorable interactions with the walls of the host cavity. Interestingly, the binding constant for **2-^{i}Pr** is lower than that for **2-Pr**, demonstrating that the binding of guests within the host cavity has a distinct dependence on guest size and shape.

van't Hoff analysis of the encapsulation of *cis*-butene complex **4** revealed the thermodynamic parameters for encapsulation for both diastereomeric host−guest assemblies of [**4** ⊂ Ga_4L_6] (Figure 3). Somewhat surprisingly, the encapsulation of **4** is slightly enthalpically disfavored, with $\Delta H_A^\circ = 1.8 \pm 0.5$ kcal/mol for the major diastereomer A and $\Delta H_B^\circ = 2.3 \pm 0.6$ kcal/mol for the minor diastereomer B. However, the binding within the supramolecular host is highly entropically favorable. For A, $\Delta S_A^\circ = 15 \pm 2$ eu, while $\Delta S_B^\circ = 15 \pm 2$ eu was determined for B (Table 5). Presumably, the release of solvent molecules, both from the solvation sphere around the unbound charged **4** and from the host cavity, provides the entropic driving force for encapsulation. These findings are consistent with previous results regarding the encapsulation of simple ammonium cations by the M_4L_6 host.[19] This behavior is reminiscent of the classical hydrophobic effect found in many entropy driven processes in biological interactions[53] and in other model host−guest systems.[54−56]

(53) Klotz, I. M. *Ligand−Receptor Energetics*; John Wiley & Sons: New York, 1997.

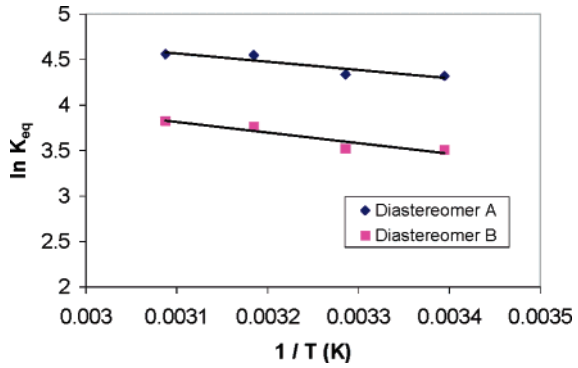

Figure 3. Plot of ln K_{eq} vs $1/T$ for the reaction of **4** (10.0 mM) and $Na_{12}[Ga_4L_6]$ (10.0 mM) in D_2O buffered with TRIS/DOTf (100.0 mM) at pD = 8.0.

Table 5. Themodynamic Parameters for the Encapsulation of **4** by $Na_{12}[Ga_4L_6]$

[**4** ⊂ Ga_4L_6]	$\Delta H°$ (kcal mol^{-1})	$\Delta S°$ (eu)
major diastereomer A	1.8(5)	15(2)
minor diastereomer B	2.3(6)	15(2)

These thermodynamic results demonstrate that both the starting and product iridium species are good guests for the supramolecular host. The initial encapsulation process is driven by the large gain in entropy resulting from the release of bound solvent molecules. In addition, the high binding affinities of these guests are also influenced by the hydrophobic ligands on the iridium metal center and the strong $\pi-\pi$ interactions with the host ligand.

Mechanistic Studies on Iridium Guest Dissociation

The highly specific substrate selectivities observed in the reaction of [**4** ⊂ Ga_4L_6] with organic substrates demonstrate that the supramolecular host is exerting precise control over the reactivity of the encapsulated iridium guest. For the observed reactions to occur within the host structure, **4** not only must be thermodynamically stable but also must remain encapsulated throughout the course of the reaction. That is, **4** cannot exchange from the host cavity into the bulk solution faster than the rate of C−H bond activation of the organic substrates, or else the reactions with organic substrates would occur outside the Ga_4L_6 cavity. Despite the strong thermodynamic binding of the iridium starting materials and products, the rate of guest dissociation for the encapsulated reactive iridium guest becomes crucial for understanding the mechanism of substrate activation. The exchange rates for a variety of guest molecules for the M_4L_6 assembly have recently been studied and have been shown to be highly dependent upon the size and shape of the encapsulated guest. While NEt_4^+ exchanges readily in minutes at room temperature, the sterically large $Cp^*_2Co^+$ guest has a very slow guest exchange rate of weeks at elevated temperatures.[28] To understand the processes governing the observed reactivity, one of our goals was to determine whether the half-sandwich iridium compounds studied would also have similarly slow rates of guest exchange.

(54) Cram, D. J.; Choi, H.-J.; Byrant, J. A.; Knobler, C. B. **1992**, *114*, 7748−7765.
(55) Meissner, R.; Garcias, X.; Mecozzi, S.; Rebek, J. J. *J. Am. Chem. Soc.* **1997**, *119*, 77−85.
(56) Cram, D. J.; Blanda, M. T.; Paek, K.; Knobler, C. B. *J. Am. Chem. Soc.* **1992**, *114*, 7765−7773.

Scheme 6. Interior Mechanism for Reaction of [**4** ⊂ Ga_4L_6] with Aldehyde Substrates

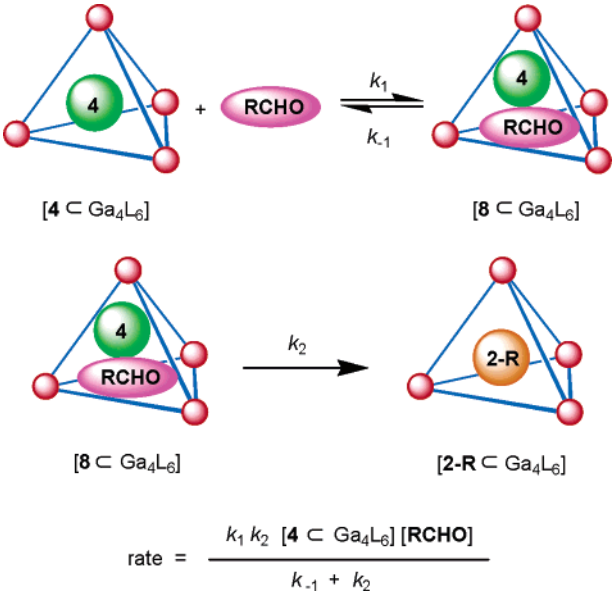

Two mechanisms for reactivity with the iridium metal center can be envisioned. In the "interior mechanism", the iridium guest **4** is strongly bound within the host cavity. An aldehyde substrate molecule (**RCHO**) of the appropriate size and shape can reversibly enter the cavity through the channels between the host walls to form substrate adduct [**8** ⊂ Ga_4L_6]. Upon entering the cavity, the substrate molecule irreversibly reacts with the iridium guest to form an encapsulated product [**2-R** ⊂ Ga_4L_6] (Scheme 6). By applying the steady-state approximation, the rate law shown in Scheme 6 can be obtained. This predicts that the reaction should be first order in both [**4** ⊂ Ga_4L_6] and **RCHO**.

Conversely, an alternative "exterior mechanism" can also be conceived. In this case, iridium complex **4** is reversibly released from the host interior. This step is the microscopic reverse of the initial encapsulation step. Once in the bulk solution, the iridium species is free to react irreversibly with the aldehyde molecule **RCHO**. Upon formation of the product, the newly formed iridium complex **2** is then encapsulated within the host (Scheme 7). Re-encapsulation is likely to be fast, since no buildup of exterior **2-R** is observed over the course of the reaction. Using the steady-state approximation, the rate law in Scheme 7 can be obtained. In this case, at sufficiently high concentrations of substrate, saturation behavior in substrate should be observed; that is, at high enough concentrations of substrate, k_2[**RCHO**] ≫ k_{-1}[Ga_4L_6]. Under these conditions, essentially every time the iridium guest exits the host cavity, it is trapped by reaction with the substrate and $k_{obs} = k_1$.

We hoped to gain better insight into this process through kinetic investigations. Unfortunately, direct quantitative kinetic studies of the C−H bond activation reactions of [**4** ⊂ Ga_4L_6] could not easily be carried out. The addition of high concentrations of organic substrates resulted in precipitation of the host−guest assembly. Therefore, we decided to indirectly investigate the mechanism of substrate activation. By utilizing sterically bulky water-soluble substrates that cannot enter the host cavity, any reactivity with the [**4** ⊂ Ga_4L_6] complex must occur via the exterior mechanism (Scheme 7). The exterior mechanism should display saturation behavior; as a result, the rate of **4**

Scheme 7. Exterior Mechanism for Reaction of [**4** ⊂ Ga_4L_6] with Aldehyde Substrates

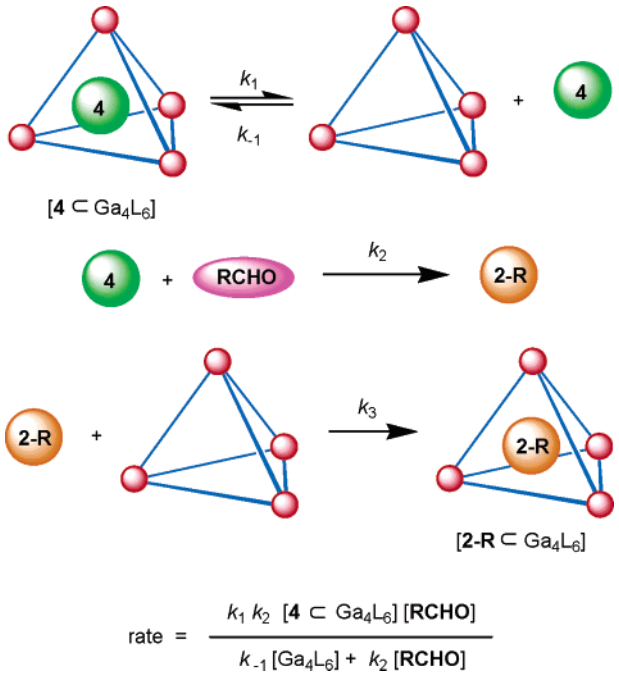

$$\text{rate} = \frac{k_1 k_2 [\mathbf{4} \subset Ga_4L_6][\mathbf{RCHO}]}{k_{-1}[Ga_4L_6] + k_2[\mathbf{RCHO}]}$$

dissociation can be determined ($k_{obs} = k_1$). Substrates that react quickly and homogeneously with **4** were desired. Ideal traps for the iridium metal center are phosphines, which react rapidly with **4** through ligand substitution of the labile *cis*-butene, resulting in iridium bis-phosphine products. There are a wide range of water-soluble phosphine ligands known,[57−59] such as triphenylphosphine tris-sulfonate sodium salt (TPPTS).[60] This ligand has been employed in the Ruhrchemie-Rhône Poulenc hydroformylation process, using biphasic conditions with a water-soluble rhodium catalyst.[61] TPPTS was an especially attractive trap for the iridium guest, as it should be too large to enter the tetrahedral host cavity. Furthermore, the electrostatic repulsion between the −11 charge on [**4** ⊂ Ga_4L_6] and the −3 charge on TPPTS should inhibit encapsulation of the phosphine.

When TPPTS was added to **4** in the absence of the Na_{12}-[Ga_4L_6] host, immediate coordination to the iridium center was observed. This reaction can be followed by the immediate color change from pale yellow to colorless. When Na_{12}[Ga_4L_6] was added to an aqueous solution of this complex, no encapsulation was observed, indicating that the iridium TPPTS complex **9** is too large to enter the host interior (Scheme 8). Thus, TPPTS coordination is fast and irreversible.

Detailed kinetic experiments were then performed on the highly active [**4** ⊂ Ga_4L_6] host−guest assembly with varying concentrations of TPPTS. A constant concentration of 10.0 mM iridium host−guest assembly was used. To control pH, the D_2O solution was buffered at pD = 8.0 using 100 mM KD_2PO_4. A constant temperature of 24 °C was used for all kinetic runs. The progress of the reaction was followed by monitoring the disappearance of diastereomers A and B of [**4** ⊂ Ga_4L_6] by ^{1}H NMR spectroscopy.

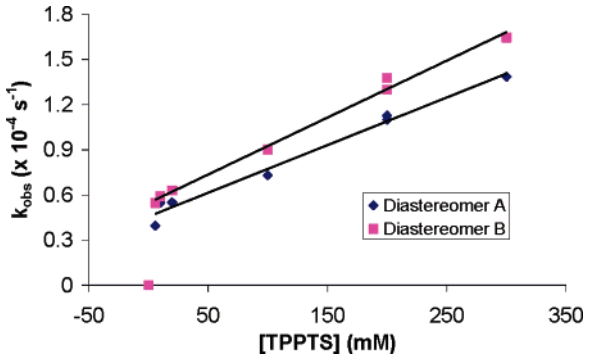

Figure 4. Plot of observed rate constant (k_{obsd}) vs [TPPTS] for the reaction of [**4** ⊂ Ga_4L_6] (10.0 mM) and TPPTS at 24.0 °C in D_2O buffered with KD_2PO_4 (100.0 mM) at pD = 8.0.

Scheme 8

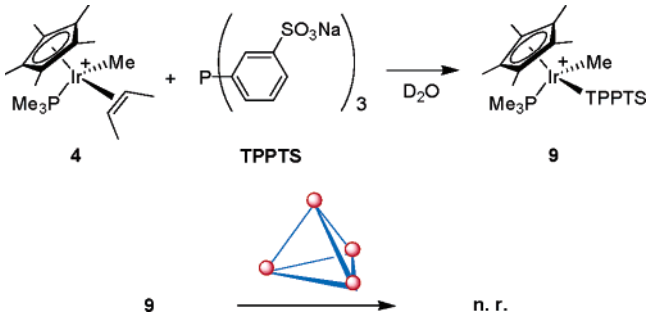

Upon addition of excess TPPTS in these reactions, the rates of disappearance of A and B are cleanly first-order but not identical. In this case, minor diastereomer B decayed faster than major diastereomer A. The rates of disappearance for both diastereomers of [**4** ⊂ Ga_4L_6] are plotted against increasing concentration of TPPTS (Figure 4). The increase in the rate for increasing concentrations of TPPTS is linear and did not appear to be approaching saturation. More significantly, the reaction did not display first order behavior in TPPTS: the observed rates do not appear to converge linearly to zero even at low concentrations of TPPTS. A control experiment with the host−guest complex and no added TPPTS was performed, which displayed no decay of [**4** ⊂ Ga_4L_6] under these conditions. This indicates that there is no background reaction involving an alternative decomposition of the host−guest assembly that would elevate the observed rates.

At low concentrations of TPPTS, the reaction should display bimolecular kinetics and a second-order decay of encapsulated guest peaks (Scheme 7). Instead, clean first-order decay in [**4** ⊂ Ga_4L_6] was observed even at low concentrations of TPPTS. This is not surprising since the rate of TPPTS coordination to the iridium center has been shown to be fast (Scheme 8), so that it is plausible that $k_2 \gg k_{-1}$. However, if the reaction exhibits this saturation behavior, then the linear increase in rate must be due to other factors in the reaction conditions besides TPPTS concentration.

At this point, other factors that might contribute to this behavior were considered. While the pH of the solution was controlled by buffering, the ionic strength of the solution was not controlled during the kinetic runs. The reaction may be sensitive to ionic species in the reaction medium.[62] At 10 mM,

(57) Joo, F. *Aqueous Organometallic Catalysis*; Kluwer: Dordrecht, 2001.
(58) *Aqueous-Phase Organometallic Catalysis. Concepts and Applications*; Wiley-VCH: Weinheim, 1998.
(59) Sinou, D. *Top. Curr. Chem.* **1999**, *206*, 41−60.
(60) Herrmann, W. A.; Kellner, J.; Riepl, H. *J. Organomet. Chem.* **1990**, *389*, 103−128.
(61) Cornils, B. *Org. Process Res. Dev.* **1998**, *2*, 121−127.
(62) Loupy, A.; Tchoubar, B. *Salt Effects in Organic and Organometallic Chemistry*; VCH: Weinheim, 1992.

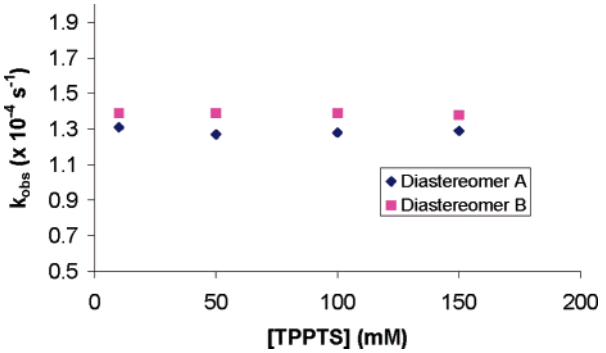

Figure 5. Plot of observed rate constant (k_{obsd}) vs [TPPTS] for the reaction of [**4** ⊂ Ga_4L_6] (10.0 mM) and TPPTS at 24.0 °C in D_2O buffered with KD_2PO_4 (100.0 mM) at pD = 8.0. Constant [Na^+] (600.0 mM) maintained by addition of NaOTf.

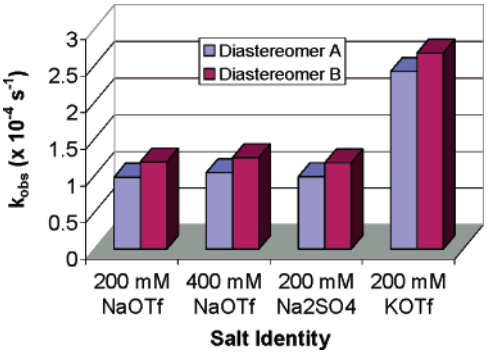

Figure 6. Graph of observed rate constant (k_{obsd}) for the reaction of [**4** ⊂ Ga_4L_6] (10 mM) and TPPTS (100 mM) at 24.0 °C in D_2O buffered with KD_2PO_4 (100 mM) at pD = 8.0 vs identities and concentrations of added salts.

the $Na_{12}[Ga_4L_6]$ host assembly contributes 120 mM Na^+ cations in solution. Since TPPTS has a −3 charge and three Na^+ counterions, the ionic strength of the solution may be greatly perturbed, especially at high TPPTS concentrations. For example, at 300 mM concentration of TPPTS, there is a 900 mM concentration of Na^+ in solution. Attempts to buffer the ionic strength of the solution using higher concentrations of chemically nonreactive salts such as 4.5 M NaOTf were unsuccessful due to precipitation of [**4** ⊂ Ga_4L_6].

To assess the effect of ionic strength on the reaction rate, a series of kinetic runs were set up as above except that a constant concentration of Na^+ was employed. When increasing amounts of TPPTS were added, the concentration of additional NaOTf was adjusted such that a total Na^+ concentration of 600 mM was maintained. No change in rate was observed despite increasing TPPTS concentrations ranging over an order of magnitude from 10 to 150 mM (Figure 5). Thus, the increase in rate due to increasing TPPTS concentration must be due solely to the increasing concentration of ions in solution. A control experiment using a constant concentration of TPPTS with additional NaOTf resulted in an acceleration of the rate of reaction (see Supporting Information). This is consistent with the observation of first-order behavior even at low concentrations of TPPTS due to the fast k_2 step.

Further Investigation of Salt Effects

In general, as the concentration of salt increases, the polarity of the solution increases (a normal salt effect),[63] and that might be expected here. Since both the host and the guest iridium species are charged, increased solvent polarity may help to separate the charged species as **4** dissociates from the cluster cavity, and this has been observed for many dissociative reactions.[64] Under dilute conditions, the Debye−Hückel limiting law relates ionic strength (I) to the component ions in solution by eq 2:

$$I = {}^1/_2 \Sigma z_i^2 m_i \qquad (2)$$

The ionic strength (I) of the solution is proportional to the sum of the square of the charges (z_i^2) and the concentrations of all the ions in solution (m_i). To probe the salt effect in this reaction, a variety of different salts were examined to identify their effect on the rate of iridium guest dissociation. If this was a normal salt effect, the rate of the reaction should depend primarily on the charges of the ions in solution rather than their character.

Changing the character of the anion was first explored. When a constant 100 mM concentration of excess TPPTS was used, the addition of 200 mM Na_2SO_4 resulted in a negligible change in the observed rate when compared to the use of 400 mM NaOTf (Figure 6). Thus, unexpectedly, the charge of the anion did not appear to affect the rate of iridium guest dissociation, despite the greater negative charge of the SO_4^{2-} anion.

Variation of the cation character was then investigated. Addition of dicationic ions such as Mg^{2+}, Ca^{2+}, and Ba^{2+} resulted in precipitation of the host assembly. Therefore, other monocationic ions were then examined. Kinetic experiments were set up as before using KOTf rather than NaOTf; the solution of [**4** ⊂ Ga_4L_6] remains homogeneous upon addition of KOTf. A normal salt effect predicts that the rates of guest dissociation should be identical for both salts. Surprisingly, the rate of the reaction with 200 mM KOTf was nearly 2 times faster than the rate observed with 200 mM NaOTf (Figure 6). Thus, the rate of iridium guest dissociation is *cation* dependent. Since the Ga_4L_6 host has a highly anionic −12 charge, it is plausible that it interacts strongly and specifically with cationic species in solution. This interaction is supported by the observation that the addition of dicationic ions precipitates the host, presumably due to strong ion pairing.

Consequently, the dependence of rate on the concentration of added KOTf was investigated. Using the conditions employed above with 100 mM excess TPPTS, varying amounts of KOTf were added and the rate of decay of [**4** ⊂ Ga_4L_6] was monitored. Similar to the results found with NaOTf, a linear increase in rate was observed upon addition of KOTf (Figure 7). However, the strength of this interaction is much larger than that seen with NaOTf. The relative magnitude of this interaction can be determined by comparing the linear slopes of Na^+ and K^+ dependence: the interaction with K^+ is approximately 4−5 times greater than the Na^+ interaction with the host−guest assembly.

The origins of this cation dependence were investigated. Guest binding studies of **4** were performed using both $Na_{12}[Ga_4L_6]$ and $K_{12}[Ga_4L_6]$ assemblies. Identical binding constants for the encapsulation of **4** were observed for both salts of the supramolecular host by ^1H NMR spectroscopy. Furthermore, addition of excess NaOTf and KOTf to Na_{11}[**4** ⊂ Ga_4L_6] did not affect guest encapsulation. As a result, the increased rate of guest dissociation observed upon addition of cations is not due to destabilization of the [**4** ⊂ Ga_4L_6] ground state. The increase

(63) Fainberg, A. H.; Winstein, S. *J. Am. Chem. Soc.* **1956**, *78*, 2763−2767.
(64) Loupy, A.; Tchoubar, B.; Astruc, D. *Chem. Rev.* **1992**, *92*, 1141−1165.

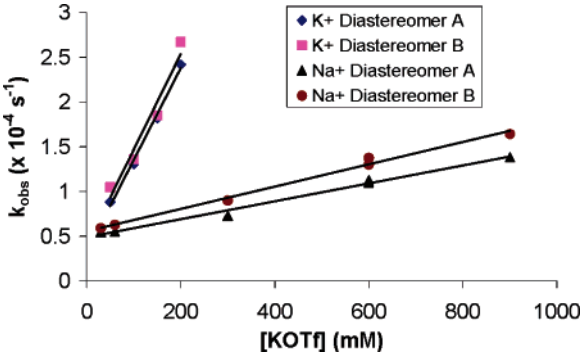

Figure 7. Plot of observed rate constant (k_{obsd}) vs [KOTf] compared to the previous results with added Na^+ for the reaction of [**4** ⊂ Ga_4L_6] (10.0 mM) and TPPTS (100.0 mM) at 24.0 °C in D_2O buffered with KD_2PO_4 (100.0 mM) at pD = 8.0.

Scheme 9

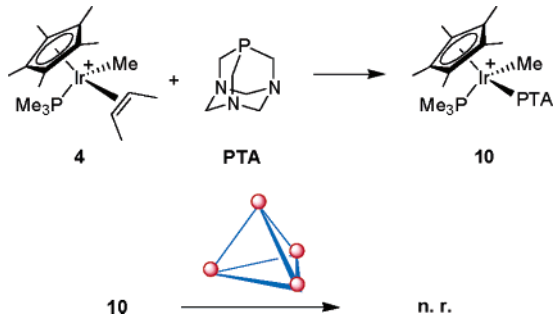

in rate is a purely kinetic phenomenon rather than a ground-state thermodynamic one.

Kinetic Investigations with a Neutral Phosphine Trap

To show that the kinetic behavior observed was general, a second water-soluble phosphine was used to trap **4**. As a complement to the anionic TPPTS ligand, the neutral 1,3,5-triaza-7-phosphaadamantane (PTA) ligand,[65,66] which has been employed in many transition metal reactions,[67−71] was investigated. In addition to being highly water soluble, the steric bulk of PTA should prevent it from entering the cavity of the host.

Upon addition of PTA to an aqueous solution of **4**, immediate PTA coordination to form **10** was observed, as with the TPPTS ligand. When the resulting iridium PTA complex **10** was added to a solution of $Na_{12}[Ga_4L_6]$, no encapsulation occurred, indicating that the guest was too large to fit within the host cavity (Scheme 9). As a result, PTA should be too large to react with the encapsulated iridium species and should give the same rate of reaction observed previously with the TPPTS ligand.

Kinetic runs were set up as above. The concentration of PTA was varied in order to determine the rate at saturation. Broad signals in the ^1H NMR spectrum for the exterior iridium complex **10** were observed to grow in over the course of the reaction. The results are plotted in Figure 8 along with the rates observed with TPPTS for comparison.

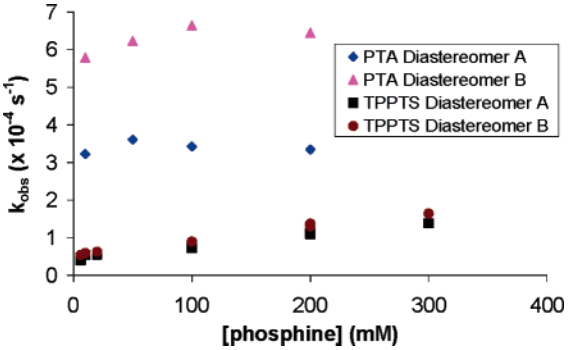

Figure 8. Plot of observed rate constant (k_{obsd}) vs [TPPTS] or [PTA] for the reaction of [**4** ⊂ Ga_4L_6] (10.0 mM) and phosphine at 24.0 °C in D_2O buffered with KD_2PO_4 (100.0 mM) at pD = 8.0.

As was observed with TPPTS at constant cation concentration, there was no significant increase in rate upon varying the concentration of PTA over an order of magnitude from 10 to 200 mM (Figure 8). This indicates that PTA does not enter the host cavity and that saturation has been achieved even at low concentrations of PTA. According to the exterior mechanism, the character of phosphine trap should not affect the observed rate of reaction (Scheme 7). Surprisingly, however, the observed rate of reaction with PTA was much higher than that with 20 mM TPPTS: the observed rate constants found were k_{PTA} = 3.40 × 10^{-4} s^{-1} and k_{TPPTS} = 0.55 × 10^{-4} s^{-1} for the major diastereomer A and k_{PTA} = 6.28 × 10^{-4} s^{-1} and k_{TPPTS} = 0.59 × 10^{-4} s^{-1} for the minor diastereomer B. In addition, the difference in rate between diastereomers A and B is much greater when trapping **4** with PTA than with TPPTS.

To explain these results, a stepwise ion pair mechanism can be conceived (Scheme 10). Ion pairing has been shown to be an important effect in many transition metal reactions.[72] Instead of **4** directly leaving the host cavity to form completely solvated species in solution, we propose that ion paired complex **11** is the initially formed intermediate. Although ion pairing is less well understood in aqueous solution, the highly anionic $[Ga_4L_6]^{12-}$ host may allow for strong electrostatic attraction with monocationic **4**. The neutral PTA ligand may then intercept this ion pair directly and coordinate to the iridium species in the k_3 step. However, the negatively charged (−3) TPPTS is electrostatically repelled by the anionic ion pair **11**. The ion pair must therefore dissociate into free ions in a k_2 equilibrium step before TPPTS can coordinate to the iridium center in the k_4 step. This results in a slower overall rate for TPPTS coordination.

We propose that Na^+ and K^+ can accelerate the reaction of [**4** ⊂ Ga_4L_6] with TPPTS by attacking the anionic ion pair **11** and directly replacing the ion-paired exterior iridium species, thus accelerating the k_2 step. Presumably, K^+ has a stronger effect than Na^+ since it is more polarizable and should be more strongly ion paired to **11**, explaining the difference in magnitude between the rates observed in the TPPTS reaction with added K^+ and Na^+. These cations, however, are too highly solvated to directly enter the host cavity. As a result, they should have no direct influence (beyond possible solvent polarity effects) on the initial k_1 step of dissociation of **4** from the host cavity. In addition, no coordination of the alkali cations to PTA was

(65) Daigle, D. J.; Peppermann, A. B.; Vail, S. L. *J. Heterocycl. Chem.* **1974**, *11*, 407−408.
(66) Daigle, D. J. *Inorg. Synth.* **1998**, *32*, 40−45.
(67) Joo, F.; Nadasdi, L.; Benyei, A. C.; Darensbourg, D. J. *J. Organomet. Chem.* **1996**, *512*, 45−50.
(68) Pruchnik, F. P.; Smolenski, P. *Appl. Organomet. Chem.* **1999**, *13*, 829−836.
(69) Darensbourg, D. J.; Joo, F.; Kannisto, M.; Katho, A.; Reibenspies, J. H.; Daigle, D. J. *Inorg. Chem.* **1994**, *33*, 200−208.
(70) Darensbourg, D. J.; Joo, F.; Kannisto, M.; Katho, A.; Reibenspies, J. H. *Organometallics* **1992**, *11*, 1990−1993.
(71) Darensbourg, D. J.; Stafford, N. W.; Joo, F.; Reibenspies, J. H. *J. Organomet. Chem.* **1995**, *488*, 99−108.
(72) Macchioni, A. *Chem. Rev.* **2005**, *105*, 2039−2073.

Scheme 10. Stepwise Ion Pair Mechanism for Guest Exchange

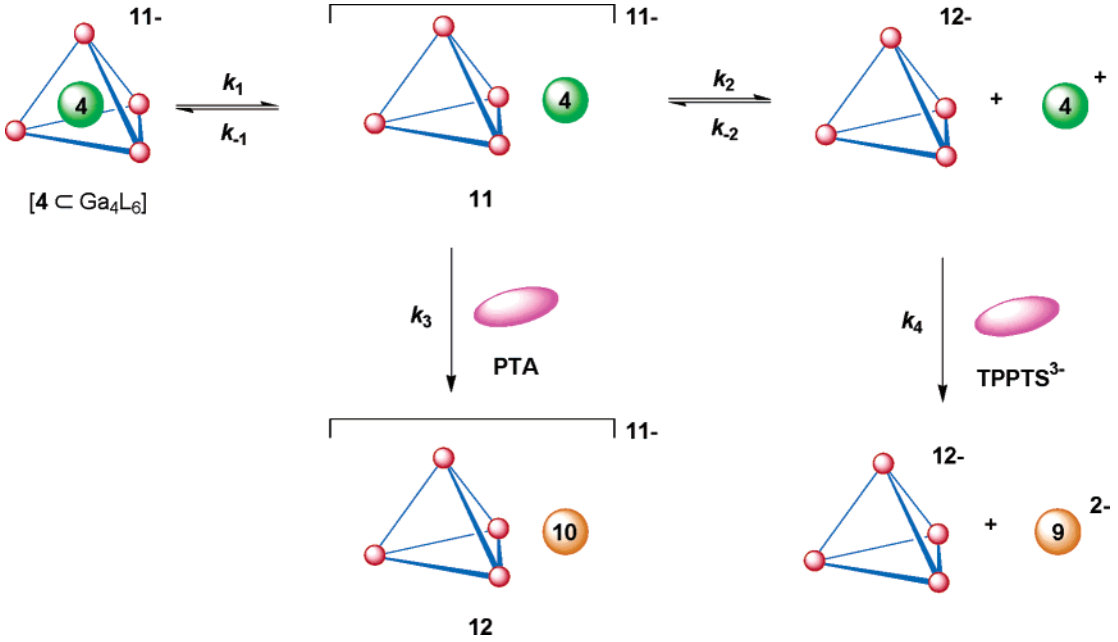

Table 6. Observed Rate Constants for the Reaction of [**4** ⊂ Ga_4L_6] (10.0 mM) with PTA (100.0 mM) in Different Solvents

[**4** ⊂ Ga_4L_6]	k_{obsd} D_2O ($\times 10^{-4}$ s^{-1})	k_{obs} CD_3OD ($\times 10^{-4}$ s^{-1})
major diastereomer A	3.42	2.60
minor diastereomer B	6.64	7.13

Table 7. Observed Rate Constants for the Reaction of [**4** ⊂ Ga_4L_6] (10.0 mM) with TPPTS (100.0 mM) in Different Solvents

[4⊂Ga_4L_6]	k_{obsd} D_2O ($\times 10^{-4}$ s^{-1})	k_{obsd} CD_3OD ($\times 10^{-4}$ s^{-1})
major diastereomer A	0.28	0.69
minor diastereomer B	0.40	1.07

observed by ^{31}P NMR spectroscopy. Consistent with this hypothesis is that addition of alkali cations, including NaOTf, KOTf, and CsOTf, has no effect on the rate of reaction of [**4** ⊂ Ga_4L_6] with PTA (see Supporting Information).

In addition to the salt effects on the ion pair **11** discussed previously, we also investigated the solvent dependence on the lifetime of **11**. The supramolecular Ga_4L_6 host is only soluble in very polar solvents such as water, methanol, DMSO, and DMF. The *cis*-butene complex **4** reacts readily with DMSO and DMF, which precluded their use in kinetic studies. However, a 3:1 mixture of CD_3OD/D_2O resulted in encapsulation of **4** with no appreciable decomposition observed. The rates of reaction were measured as above with either 100 mM of PTA or TPPTS. No significant solvent effect was observed with the PTA reaction (Table 6). The solvent apparently does not play a large role in the initial dissociation of **4** from the host cavity in the k_1 step (Scheme 10).

However, there is a significant acceleration of the TPPTS reaction in methanolic solution (Table 7). In this case, methanol appears to decrease the lifetime of **11**, allowing the TPPTS ligand to react with fully dissociated **4** at a much faster rate. One possible explanation for this result is that water provides a tighter hydrogen-bonded solvent cage around the iridium−host ion pair, inhibiting iridium ion pair dissociation. Methanol, in contrast, provides a weaker solvent cage, and **4** is allowed to dissociate from the ion pair **11** at a much faster rate. Such effects have been observed in radical reactions and even some ionic reactions.[73,74]

Having obtained kinetic evidence for the existence of ion pair **11** in our guest dissociation studies, we sought to directly detect the existence of this ion pair. ^1H NOESY NMR spectroscopy has been used previously to obtain characterization of ion pairs in solution,[75−84] so we hoped to detect the existence of ion pair **11** by this method. As discussed previously, upon addition of **4** to $Na_{12}[Ga_4L_6]$, the remaining exterior **4** exhibited broad ^1H NMR resonances. The Cp* resonances are shifted upfield by 0.5 ppm and overlay the resonances for the PMe_3 peaks. This is an indication of potential π-stacking interactions between the external iridium Cp* moiety and the naphthalene ligand of the host assembly, resulting in a slight upfield shift of the Cp* NMR resonances. Addition of 1 equiv of the strongly binding NEt_4^+ ($K_{eq} = 196 \times 10^2$ M^{-1})[19] displaces the encapsulated **4**, resulting in large broad exterior peaks for **4**. Unfortunately, NOE studies performed on this ion pair yielded no results. Without the

(73) Braden, D. A.; Parrack, E. E.; Tyler, D. R. *Coord. Chem. Rev.* **2001**, *211*, 279−294.
(74) Warrick, P.; Auborn, J. J.; Eyring, E. M. *J. Phys. Chem.* **1972**, *76*, 1184−1191.
(75) Pochapsky, T. C.; Stone, P. M. *J. Am. Chem. Soc.* **1990**, *112*, 6714−6715.
(76) Pochapsky, T. C.; Wang, A. P.; Stone, P. M. *J. Am. Chem. Soc.* **1993**, *115*, 11084−11091.
(77) Bellachioma, G.; Cardaci, G.; Macchioni, A.; Reichenbach, G.; Terenzi, S. *Organometallics* **1996**, *15*, 4349−4351.
(78) Macchioni, A.; Bellachioma, G.; Cardaci, G.; Gramlich, V.; Ruegger, H.; Terenzi, S.; Venanzi, L. M. *Organometallics* **1997**, *16*, 2139−2145.
(79) Bellachioma, G.; Cardaci, G.; Gramlich, V.; Macchioni, A.; Valentini, M.; Zuccaccia, C. *Organometallics* **1998**, *17*, 5025−5030.
(80) Macchioni, A.; Bellachioma, G.; Cardaci, G.; Cruciani, G.; Foresti, E.; Sabatino, P.; Zuccaccia, C. *Organometallics* **1998**, *17*, 5549−5556.
(81) Bellachioma, G.; Cardaci, G.; Macchioni, A.; Zuccaccia, C. *J. Organomet. Chem.* **2000**, *2000*, 593−594.
(82) Dupont, J.; Suarez, P. A. Z.; De Souza, R. F.; Burrow, R. A.; Kintzinger, J.-P. *Chem.—Eur. J.* **2000**, *6*, 2377−2381.
(83) Zuccaccia, C.; Stahl, N. G.; Macchioni, A.; Chen, M.-C.; Roberts, J. A.; Marks, T. J. *J. Am. Chem. Soc.* **2004**, *126*, 1448−1464.
(84) Beringhelli, T.; D'Alfonso, G.; Maggioni, D.; Mercandelli, P.; Sironi, A. *Chem.—Eur. J.* **2005**, *11*, 650−661.

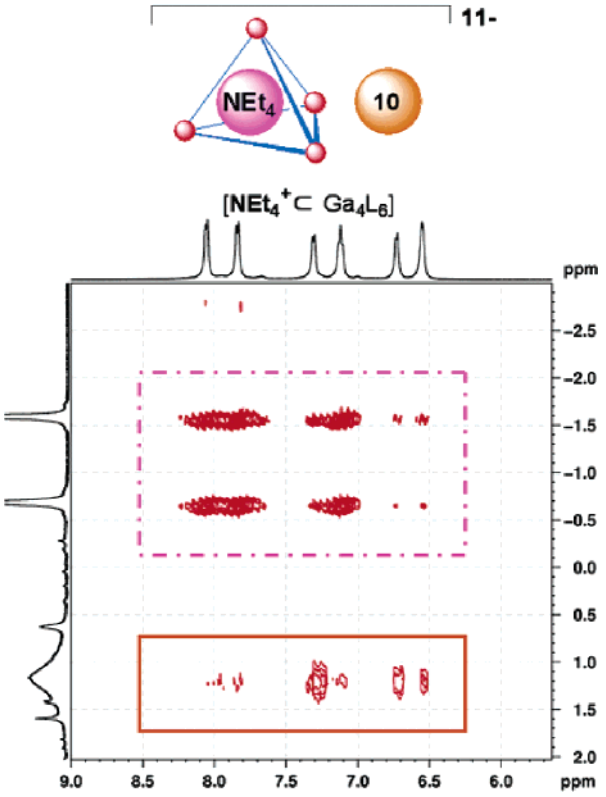

Figure 9. Selected ^{1}H NOESY spectrum of exterior **10** in ion pair with [$NEt_4^+ \subset Ga_4L_6$]. The purple dashed box highlights correlations between encapsulated NEt_4^+ with the three symmetry equivalent Ga_4L_6 host naphthyl protons. The orange solid box highlights correlations between broad exterior Cp* peaks for **10** at 1 ppm and the three symmetry equivalent Ga_4L_6 host catecholate protons.

stabilization of encapsulation, **4** decomposes over the time scale of the experiment.

While **4** is only transiently ion-paired to the exterior of the host assembly before being trapped by the PTA ligand, due to its similar charge, the resulting PTA complex **10** may also form ion pair **12** with the Ga_4L_6 host (Scheme 10). Evidence for the existence of **12** would support our hypothesis of ion pairing in the preceding intermediate. The peaks for exterior **10** in the presence of the host assembly are also broad in the ^{1}H NMR spectrum. Ion pair **12** consists of iridium PTA complex **10** on the exterior of the formally empty Ga_4L_6 host. In the absence of a guest, the empty host is unstable over long periods of time, so 1 equiv of the strongly binding guest NEt_4^+ was added in order to stabilize the empty Ga_4L_6 host. The ^{1}H NMR resonances for **10** remained as broad signals, reflecting its continued binding to the exterior of the host assembly. A ^{1}H NOESY spectrum of this solution was obtained, utilizing a short mixing time appropriate for high molecular weight species to rule out possible diffusion artifacts (Figure 9). As expected, NOE cross-peaks were observed with the encapsulated NEt_4^+ guest and the Ga_4L_6 host proton resonances. The strongest correlations are those between the guest and the naphthalene protons; this is expected, since the encapsulated guest is sandwiched within the naphthalene walls of the host assembly.

Interestingly, PTA complex **10** also displayed NOE correlations with the host resonances, showing that **10** and the Ga_4L_6 host lie in close proximity to each other in solution. This is strong evidence that an ion pair exists between the external iridium species and the supramolecular host in **12**. In this case, the NOE cross-peaks with the catecholate protons at the corners of the tetrahedron are more intense than the naphthalene protons at the sides of host. This is most likely due to the fact that the anionic charge on the $Ga_4L_6^{12-}$ host is concentrated at the metal catecholate vertices of the assembly. Electrostatic attraction to monocationic **10** therefore results in strong ion pairing to the corners of the host structure.

The strength of this ion pairing effect was investigated. Upon addition of 10 equiv of NMe_4^+, NOE correlations are still observed between **10** and the host assembly. Although NMe_4^+ has a strong interaction with the exterior of the Ga_4L_6 assembly,[85] a 10-fold greater concentration of NMe_4^+ is incapable of displacing the ion-paired iridium species. Evidence from X-ray diffraction studies have shown that exterior ammonium cations such as NEt_4^+ bind strongly with the naphthalene faces of the ligand scaffold through π-cation interactions, which may allow the strong electrostatic attraction between **10** and the catecholate corners of the host to continue.[15]

In contrast to the result with **10**, the ^{1}H NMR resonances for the exterior TPPTS complex **9** are sharp. The Cp* and PMe_3 proton resonances are cleanly separated, with the Cp* resonance at ~2 ppm. A ^{1}H NOESY experiment showed no correlations between the anionic **9** and the supramolecular host. While this lack of ion pairing only probes the interactions of the TPPTS product **9** with the Ga_4L_6 host, it strongly suggests a lack of ion pairing in the preceding reaction intermediate (Scheme 10). Thus, the broad peaks corresponding to resonances for exterior iridium species **10** indicate the formation of ion pair aggregates in solution.

Energies of Ion Pair Formation and Dissociation

In the ion pair mechanism for guest dissociation, the rate-limiting step in the trapping of **4** with the neutral PTA ligand should be the initial ion pair formation step, k_1 (Scheme 10). On the other hand, the rate-limiting step in the case of the anionic TPPTS trap is the ion pair dissociation step, k_2. Since both rate constants k_1 and k_2 can be accessed by kinetic analysis using the different phosphine traps, an Eyring study was performed to obtain activation parameters for both ion pair formation and dissociation. To eliminate the effects of alkali cations in solution, 100 mM Tris/DOTf buffer at pD = 8.0 was used instead of KD_2PO_4.

The rate of reaction of [**4** ⊂ Ga_4L_6] with PTA was monitored at several different temperatures, producing a linear Eyring plot (Figure 10). The activation parameters for both diastereomers can be obtained (Table 8). These parameters translate into a standard free energy $\Delta G_{298}^{\ddagger}$ of 22.3 ± 1.3 kcal/mol for major diastereomer A, higher than the barrier of 21.7 ± 1.3 kcal/mol for B. The difference between these activation energies accounts for the difference in the rate of reaction between the two diastereomeric host−guest assemblies observed upon addition of PTA.

An Eyring study was then performed with the TPPTS ligand (Figure 11). Since the reaction of [**4** ⊂ Ga_4L_6] with TPPTS proceeds via both the formation and dissociation steps of ion pair **11**, Eyring analysis yields the overall activation parameters for both the k_1 and k_2 steps of the proposed mechanism. To deconvolute the activation parameters for the k_2 ion pair dissociation step, the thermodynamic equilibrium parameters

(85) Michels, M.; Raymond, K. N. Unpublished results.

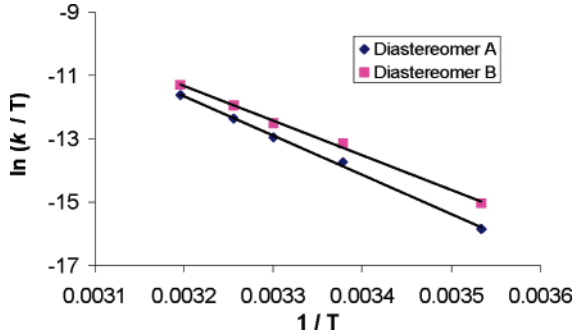

Figure 10. Plot of ln(k /T) vs 1/T for the reaction of [**4** ⊂ Ga_4L_6] (10.0 mM) and PTA (100.0 mM) at 24.0 °C in D_2O buffered with KD_2PO_4 (100.0 mM) at pD = 8.0.

Table 8. Observed Activation Parmeters for the Stepwise Guest Exchange Reaction of [**4** ⊂ Ga_4L_6] (10.0 mM)

[**4** ⊂ Ga_4L_6]	$\Delta H^{\ddagger}$ (k_{cald} mol^{-1})	$\Delta S^{\ddagger}$ (eu)
k_1 diastereomer A	24.7(7)	8(2)
k_1 diastereomer B	21.7(7)	0(2)
k_2 diastereomer A	22(1)	6(5)
k_2 diastereomer B	22(2)	4(5)

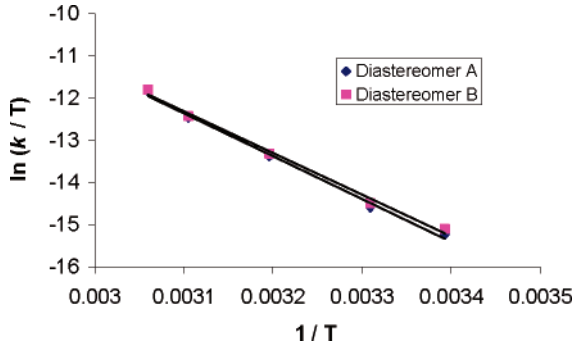

Figure 11. Plot of ln(k/T) vs 1/T for the reaction of [**4** ⊂ Ga_4L_6] (10.0 mM) and TPPTS (100.0 mM) at 24.0 °C in D_2O buffered with KD_2PO_4 (100.0 mM) at pD = 8.0.

between [**4** ⊂ Ga_4L_6] and ion pair **11** must be known. Since only a negligible amount of free **4** is observed in solution, the previously observed van't Hoff equilibrium parameters for the encapsulation of **4** mainly concern the equilibrium between ion pair **11** and [**4** ⊂ Ga_4L_6]. However, both ion pair **11** and [**4** ⊂ Ga_4L_6] exist as diastereomeric pairs A and B. The van't Hoff study only establishes the difference in ground-state energies between ion pair **11** and [**4** ⊂ Ga_4L_6]; it is unknown whether this difference in ground-state energies between the major diastereomer A and the minor diastereomer B occurs in either **11** or [**4** ⊂ Ga_4L_6].

Since the thermodynamic stabilities of the ion pair **11** and [**4** ⊂ Ga_4L_6] have been determined, the activation parameters for only the k_2 step can be isolated (Table 8). At 298 K, the free energy change associated with ion pair dissociation has $\Delta G_{298}^{\ddagger} = 20.2 \pm 2.8$ kcal/mol for A and $\Delta G_{298}^{\ddagger} = 20.5 \pm 3.0$ kcal/mol for B. This explains the differences in the rate of reaction of the two diastereomers A and B with PTA and TPPTS. In contrast to the barriers for ion pair formation, the magnitudes of the barriers for ion pair dissociation for each diastereomer are reversed: A has a lower activation barrier than B. As a result, the difference in the rates of disappearance of both A and B when trapping with TPPTS is very small, since the diastereoselectivity of the k_2 step opposes that of the k_1 step.

Combining these results, a complete free energy coordinate diagram can be described for the guest dissociation of both diastereomers of [**4** ⊂ Ga_4L_6] (Figure 12). Since it is unknown whether the difference in ground-state energy between the two diastereomers occurs for [**4** ⊂ Ga_4L_6] or ion pair **11**, both diastereomers for [**4** ⊂ Ga_4L_6] are drawn at the same relative energy so that the overall reaction coordinates can be compared. The highest overall potential barrier for guest exchange into the bulk solution is ion pair dissociation k_2, which explains the slower saturation rate constant for TPPTS. This demonstrates the strength of the ion pairing interaction.

While ion pairing interactions play important roles in biological processes, the study of ion pair intermediates in aqueous solutions has largely been limited to solvolysis reactions.[86,87] However, this stepwise model for guest dissociation in aqueous solution appears to be general for this system. Fiedler et al. have found evidence for a similar ion pair intermediate in the guest exchange of reactive iminium cations from the Ga_4L_6 host.[88] Davis et al. have also shown evidence of ion pairing effects in the rate of guest exchange of simple ammonium cations.[29]

Both the k_1 and k_2 steps are significantly slower than the rate observed in the C−H bond activation of aldehdyes, which takes place quantitatively in 30 min at room temperature. The rate of saturation of the TPPTS reaction with [**4** ⊂ Ga_4L_6] has a $t_{1/2}$ of ~3.5 h in the absence of added salt, while the rate of saturation of the PTA reaction with [**4** ⊂ Ga_4L_6] has a $t_{1/2}$ of ~30 min. This is the upper limit at which **4** dissociates from the host cavity to form the exterior ion pair **11**. Since the C−H bond activation of aldehydes occurs more rapidly ($t_{1/2}$ ~5 min), this reaction must occur within the host cavity. However, since **4** does dissociate from the host, reaction with bulky organic substrates should be observed, with a rate at saturation equivalent to that of the reaction of [**4** ⊂ Ga_4L_6] with PTA. Indeed, upon addition of 50 mM benzaldehyde to 10 mM [**4** ⊂ Ga_4L_6], formation of exterior **2-Ph** (confirmed by ^1H, $^{31}P\{^1H\}$, $^{13}C\{^1H\}$ NMR and IR spectroscopy) was observed over a period of 24 h. This rate is much slower than the rate of reaction of [**4** ⊂ Ga_4L_6] with acetaldehyde and PTA. This rate is consistent with **4** slowly dissociating from the host and reacting with benzaldehyde. Unfortunately, saturation kinetics in benzaldehyde could not be obtained since higher concentrations of benzaldehyde led to precipitation of the host−guest assembly. As a result, the high level of size and shape substrate selectivity is due to the well-defined cavity of the Ga_4L_6 host, achieved due to truly supramolecular control over reactivity.

Conclusion

The results reported here demonstrate the ability of a supramolecular host to act as a nanoscale molecular capsule for the functional encapsulation of reactive organometallic guests. Upon encapsulation within the well-defined cavity of the $Na_{12}[Ga_4L_6]$ host, highly specific size and shape selectivities are observed in the C−H bond activation reactions of aldehydes and ethers. Mechanistic studies have established that the reactive iridium guests and their products are bound strongly by the host

(86) Tsuji, Y.; Toteva, M. M.; Garth, H. A.; Richard, J. P. *J. Am. Chem. Soc.* **2003**, *125*, 15455−15465.
(87) Tsuji, Y.; Richard, J. P. *Chem. Rec.* **2005**, *5*, 94−106.
(88) Fiedler, D.; van Halbeek, H.; Bergman, R. G.; Raymond, K. N. Submitted, 2006.

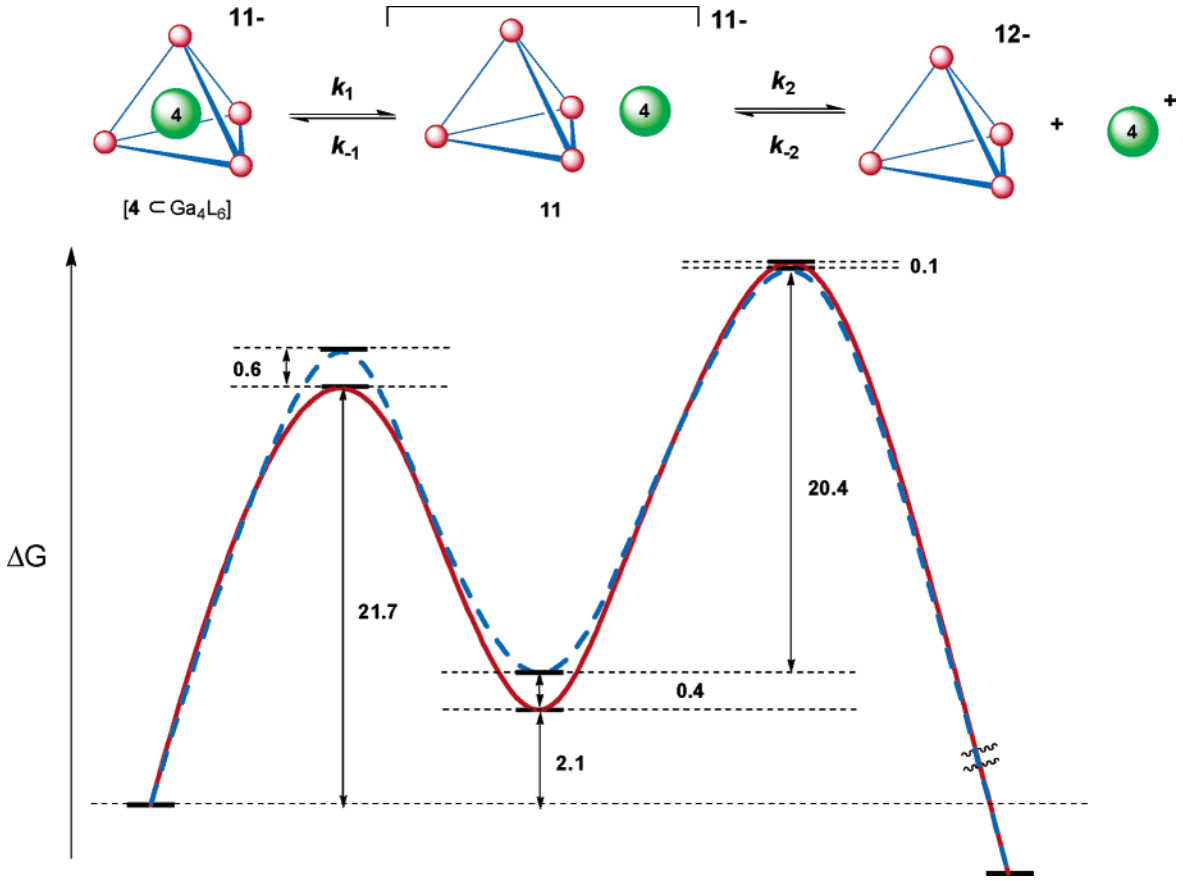

Figure 12. Energy coordinate diagram for stepwise dissociation of **4** from Ga_4L_6 host proceeding through ion pair intermediate **11** at 298 K. The blue dashed line indicates the major diastereomer A, and the red line represents the minor diastereomer B. Since both [**4** ⊂ Ga_4L_6] and ion pair **11** are diastereomeric, it is unknown where the difference in ground-state energy occurs. Both diastereomers are drawn starting from the same relative energy. Units are in kcal/mol.

cavity. Kinetic studies have revealed a novel stepwise iridium guest dissociation mechanism that proceeds via a strongly bound ion pair intermediate. This guest dissociation is slower than the rate of C−H bond activation, indicating that the reactions with the encapsulated guest occur within the cavity of the host. It is the well-defined microenvironment of the supramolecular host that dictates both the reactivity of the guest and the high substrate selectivity. This is a rare example of a fully characterized supramolecular host−guest complex in which organometallic chemistry has been directly observed to take place at a metal center sequestered within the cavity of the host and shows great promise for the future development of selective supramolecular catalysts.

Experimental Section

General. Unless otherwise noted, reactions and manipulations were carried out under inert atmosphere by using standard Schlenk and vacuum techniques or in a Vacuum Atmospheres inert atmosphere glovebox (N_2) at ambient temperature. ^{1}H, ^{13}C{^{1}H}, ^{31}P{^{1}H}, ^{19}F, and ^{2}H NMR spectra were recorded at 500, 125, 203, 376, and 77 MHz, respectively on a Bruker DRX-500, AV-500, or AVQ-400 spectrometer. All NMR chemical shifts are reported as δ in parts per million (ppm). ^{1}H and ^{13}C{^{1}H} NMR spectra are reported relative to residual solvent. ^{31}P{^{1}H} NMR spectra are reported relative to trimethyl phosphate as the external standard. ^{19}F NMR spectra are reported relative to $CFCl_3$ as the external standard. Coupling constants are reported in Hz. Suitable ^{13}C{^{1}H} NMR spectra of transition metal host−guest complexes could not be obtained after 4000 scans with a prescan delay set to 10 s. Electrospray mass spectrometric analyses (ESI-MS) were obtained at the University of California−Berkeley Mass Spectrometry facility on a triple quadrupole VG Quattro mass spectrometer. High-resolution TOF electrospray mass spectra (TOF MS ES) were recorded at the Waters facility in Dublin, CA, on a Waters QTOF API mass spectrometer equipped with a Z-spray source. Elemental analyses (EA) were performed by the Microanalytical Laboratory in the College of Chemistry at the University of California, Berkeley. Since an indeterminate amount of solvent and acetone (from workup) remains fixed to the exterior of the cluster, suitable elemental analyses of the host−guest complexes could not be obtained.

All reagents were used as received from commercial suppliers unless otherwise noted. Anhydrous solvents were passed through a column of activated alumina (type A2, size 12 × 32, Purify) under nitrogen pressure and sparged with nitrogen before use.[89] Deuterated solvents were purchased from Cambridge Isotope Laboratories and were either vacuum transferred from CaH_2 or degassed by three freeze−pump−thaw cycles and placed over activated 4 Å molecular sieves under an inert atmosphere. Water and deuterated water were sparged with nitrogen for 30 min to remove oxygen and stored under inert atmosphere. The compounds H_4L and $Na_{12}[Ga_4L_6]$ were prepared using a procedure previously developed by Raymond and co-workers.[12] The compound Cp*(PMe_3)Ir(Me)(OTf)[42] was prepared using a procedure developed by Bergman and co-workers. [Cp*(PMe_3)Ir(Me)(C_2H_4)][OTf] (**1**)[23] was prepared as previously reported. The reactions and product characterization of Cp*(PMe_3)Ir(Me)(OTf) with aldehydes,[44,45] ethers,[44,48] cyclopropane,[42,44] and dihydrogen[44,49] have been reported previously. The formation and characterization of Na_{11}[Cp*(PMe_3)Ir(CO)(R) ⊂ Ga_4L_6] encapsulated products of aldehyde activation have

(89) Alaimo, P. J.; Peters, D. W.; Arnold, J.; Bergman, R. G. *J. Chem. Educ.* **2001**, *78*, 64.

been previously reported.[23] The phosphine ligand 1,3,5-triaza-7-phospha-adamantane (TPA)[65,66] was prepared according to literature methods. For experiments with gaseous reagents, NMR tubes fitted with Teflon stopcocks (J. Young tubes) were used.

[Cp*(PMe$_3$)Ir(Me)(propene)][OTf] (3). A 100-mL Schlenk flask in the glovebox was charged with a magnetic stir bar and Cp*(PMe$_3$)-Ir(Me)(OTf) (~500 mg, 0.88 mmol) as a solid. This was dissolved in 15 mL of CH_2Cl_2. The Schlenk flask was removed from the glovebox and placed through three freeze−pump−thaw cycles on a vacuum line before being backfilled with 1 atm of propene gas. The solution was shaken briefly. The color immediately turned from deep orange to pale yellow. The solution was stirred overnight at room temperature. **3** was isolated by removing solvent in vacuo to leave a yellow oil. Trituration with Et_2O resulted in the formation of a yellow powder that was stored in the glovebox under N_2 at −30 °C. Products were isolated as a mixture of two diastereomers A and B, with a dr of 74:26. Yield: 521 mg (97%). ^{1}H NMR (CD_2Cl_2): δ 2.94 (m, 1H, *alkenyl*, A), 2.84 (m, 1H, *alkenyl*, B), 2.51 (m, 1H, *alkenyl*, B), 2.43 (m, 1H, *alkenyl*, A), 2.30 (m, 1H, *alkenyl*, A), 2.06 (m, 1H, *alkenyl*, B), 1.77 (d, J_{P-H} = 2.0 Hz, 15H, $C_5(CH_3)_5$ A), 1.68 (d, J_{P-H} = 1.5 Hz, 15H, $C_5(CH_3)_5$ B), 1.50 (m, 12H, $P(CH_3)_3$ B and *alkenyl* CH_3 A), 1.35 (d, J_{P-H} = 10.6 Hz, 9H, $P(CH_3)_3$ A), 1.15 (d, J = 6.0 Hz, 3H, *alkenyl* CH_3 B), 0.82 (d, J_{P-H} = 6.6 Hz, 3H, CH_3 A), 0.46 (d, J_{P-H} = 7.3 Hz, 3H, CH_3 B). ^{13}C{^{1}H} NMR (CD_2Cl_2): δ 101.0 (d, J_{P-C} = 2 Hz, $C_5(CH_3)_5$ A), 101.0 (br s, $C_5(CH_3)_5$ B), 58.9 (s, CH_2 A), 51.8 (s, CH_2 B), 40.1 (s, *C*H A), 37.5 (s, *C*H B), 17.3 (s, *propene* CH_3 A), 15.7 (s, *propene* CH_3 B), 14.1 (d, J_{P-C} = 42 Hz, $P(CH_3)_3$ B), 11.2 (d, J_{P-C} = 42 Hz, $P(CH_3)_3$ A), 9.0 (s, $C_5(CH_3)_5$ A), 8.2 (s, $C_5(CH_3)_5$ B), −16.0 (d, J_{P-C} = 10 Hz, CH_3 B), −16.9 (d, J_{P-C} = 10 Hz, CH_3 A). ^{31}P{^{1}H} NMR (CD_2Cl_2): δ −28.1 (s, $P(CH_3)_3$ A), −32.1 (s, $P(CH_3)_3$ B). ^{19}F NMR (CD_2Cl_2): δ −78.1 (s, OSO_2CF_3). Anal. Cald for $C_{18}H_{33}SF_3O_3PIr$: C, 35.46; H, 5.46; S, 5.26. Found: C, 35.48; H, 5.45; S, 5.00.

[Cp*(PMe$_3$)Ir(Me)(*cis*-butene)][OTf] (4). A 100-mL Schlenk flask in the glovebox was charged with a magnetic stir bar and Cp*(PMe$_3$)-Ir(Me)(OTf) (~500 mg, 0.88 mmol) as a solid. This was dissolved in 15 mL of CH_2Cl_2. The Schlenk flask was removed from the glovebox and placed through three freeze−pump−thaw cycles on a vacuum line before being backfilled with 1 atm of *cis*-butene gas. The solution was shaken briefly. The color immediately turned from deep orange to pale yellow. The solution was stirred overnight at room temperature. **4** was isolated by removing solvent in vacuo to leave a yellow oil. Trituration with Et_2O resulted in the formation of a yellow powder that was stored in the glovebox under N_2 at −30 °C. Yield: 491 mg (89%). ^{1}H NMR (CD_2Cl_2): δ 5.45 (m, 2H, *alkenyl*), 1.72 (d, J_{P-H} = 4.9 Hz, 15H, $C_5(CH_3)_5$), 1.59 (m, 9H, $P(CH_3)_3$), 1.39 (d, J = 10.4 Hz, 6H, $C_2H_2(CH_3)_2$), 0.82 (br, 3H, CH_3). ^{13}C{^{1}H} NMR (CD_2Cl_2): δ 101.4 (s, $C_5(CH_3)_5$), 57.9 (br s, $CH(CH_3)$), 13.0 (br s, *butene* CH_3), 11.4 (d, J_{P-C} = 42 Hz, $P(CH_3)_3$), 8.8 (s, $C_5(CH_3)_5$), −15.8 (d, J_{P-C} = 9 Hz, CH_3). ^{31}P{^{1}H} NMR (CD_2Cl_2): δ −26.8 (s, $P(CH_3)_3$). ^{19}F NMR (CD_2Cl_2): δ −78.1 (s, OSO_2CF_3). Anal. Cald for $C_{19}H_{35}S\ F_3O_3PIr$: C, 36.59; H, 5.66; S, 5.14. Found: C, 36.37; H, 5.49S, 5.15.

[Na$_2$][Cp*(PMe$_3$)Ir(Me)(TPPTS)] (9). In the glovebox, a 20-mL scintillation vial was charged with Cp*(PMe$_3$)Ir(Me)(OTf) (50 mg, 0.088 mmol) suspended in 5 mL of H_2O. A stoichiometric amount of TPPTS (51 mg, 0.088 mmol) was added as a solid, and the solution was stirred overnight until a colorless solution was obtained. The solvent was removed by lyophilization to give a white, air-stable powder. This was isolated as the hexa-aquo species, as determined by ^{1}H NMR in CD_3OD and elemental analysis. Yield: 93 mg (92%). The carbon α to the phosphorus in the TPPTS ligand was detected by a ^{31}P−^{13}C heteronuclear single and multiple bond correlation experiment with ^{1}H-decoupling in both dimensions on a Bruker AV-500 spectrometer equipped with a triple resonance inverse broadband probe. The experiment is optimized for coupling constants (^{31}P−^{13}C) at 10 Hz. ^{1}H NMR (D_2O): δ 7.93 (m, 6H, *aryl*), 7.57 (m, 3H, *aryl*), 7.41 (m, 3H, *aryl*), 1.50 (m, 15H, $C_5(CH_3)_5$), 1.15 (d, J_{P-H} = 10.0 Hz, 9H, $P(CH_3)_3$), 0.52 (m, 3H, CH_3). ^{1}H NMR (CD_3OD): δ 4.88 (s, 12H, 6H_2O). ^{13}C-{^{1}H} NMR (D_2O): δ 143.8 (d, J_{P-C} = 11 Hz, *meta aryl* *C*−SO_3Na), 136.6 (m, *ortho aryl* *C*H−C−SO_3Na), 132.5 (d, J_{P-C} = 15 Hz, *ortho* *C*−H *aryl*), 130.2 (d, J_{P-C} = 8 Hz, *meta* *C*−H *aryl*), 128.7 (s, *para* *C*−H *aryl*), 99.8 (m, $C_5(CH_3)_5$), 15.6 (d, J_{P-C} = 40 Hz, $P(CH_3)_3$), 8.7 (s, $C_5(CH_3)_5$), −26.5 (m, CH_3). ^{31}P−^{13}C HSMBC (D_2O): δ 132.3 (d, J_{P-C} = 50.8 Hz, P−*C aryl*). ^{31}P{^{1}H} NMR (D_2O): δ 1.0 (d, J_{P-P} = 17.8 Hz, *TPPTS*), −44.9 (d, J_{P-P} = 17.8 Hz, $P(CH_3)_3$). ^{19}F NMR (D_2O): δ −78.1 (s, OSO_2CF_3). Anal. Cald for $C_{33}H_{39}S_4F_3O_{12}P_2IrNa_3$ + 6H_2O: C, 31.86; H, 4.13; S, 10.31. Found: C, 31.90; H, 3.90; S, 9.93.

[Cp*(PMe$_3$)Ir(Me)(PTA)][OTf] (10). In the glovebox, a 20-mL scintillation vial was charged with Cp*(PMe$_3$)Ir(Me)(OTf) (50 mg, 0.088 mmol) suspended in 5 mL of H_2O. A stoichiometric amount of PTA (14 mg, 0.088 mmol) was added as a solid, and the solution was stirred overnight until a colorless solution was obtained. The solution was then lyophilized to give a white, air-stable powder. Yield: 53 mg (83%). ^{1}H NMR (D_2O): δ 4.52 (m, 6H, PCH_2N), 4.08 (s, 6H, NCH_2N), 1.87 (m, 15H, $C_5(CH_3)_5$), 1.60 (d, J = 10.4 Hz, 9H, $P(CH_3)_3$), 0.17 (m, 3H, CH_3). ^{13}C{^{1}H} NMR (D_2O): δ 98.9 (m, $C_5(CH_3)_5$), 71.2 (d, J_{P-C} = 6 Hz, NCH_2N), 49.7 (d, J_{P-C} = 22 Hz, PCH_2N), 17.5 (d, J_{P-C} = 41 Hz, $P(CH_3)_3$), 9.4 (s, $C_5(CH_3)_5$), −31.8 (m, CH_3). ^{31}P{^{1}H} NMR (D_2O): δ −44.7 (d, J_{P-P} = 21.1 Hz, $P(CH_3)_3$), −77.9 (d, J_{P-P} = 21.1 Hz, *PTA*). ^{19}F NMR (D_2O): δ −78.1 (s, OSO_2CF_3). Anal. Cald for $C_{21}H_{39}N_3SF_3O_3P_2Ir$: C, 34.80; H, 5.42; N, 5.80; S, 4.42. Found: C, 34.54; H, 5.61; N, 5.81; S, 4.26.

Na$_{11}$[3 ⊂ Ga$_4$L$_6$]. In the glovebox, an NMR tube was charged with **3** (~3 mg, 5 × 10^{-3} mmol) as a solid. This was dissolved in 0.5 mL of D_2O to give a pale yellow solution. A stoichiometric amount of $Na_{12}[Ga_4L_6]$ (~18 mg, 5 × 10^{-3} mmol) was added as a solid to form a bright yellow solution. The NMR tube was then removed from the glovebox and flame-sealed under a static vacuum on a high vacuum Schlenk line. Three diasteomeric host−guest complexes A, B, and C were observed with a dr of 50:40:10. ^{1}H NMR (D_2O): δ 8.15 (br s, *aryl*), 7.56 (br s, *aryl*), 7.38 (d, J = 8.4 Hz, *aryl*), 7.17 (d, J = 8.4 Hz, *aryl*), 6.83 (d, J = 7.6 Hz, *aryl*), 6.76 (d, J = 8.4 Hz, *aryl*), 6.73 (m, *aryl*), 3.41 (m, 3H, *alkenyl* C*H* C), 3.38 (m, 3H, *alkenyl* C*H* B), 3.33 (m, 3H, *alkenyl* C*H* A), 0.15, (m, 3H, *alkenyl* CH_3 A), −0.25 (d, J = 6.4 Hz, 3H, *alkenyl* CH_3 B), −0.33 (d, J_{P-H} = 2.0 Hz, 15H, $C_5(CH_3)_5$ A), −0.34 (d, J_{P-H} = 2.0 Hz, 15H, $C_5(CH_3)_5$ B), −0.46 (d, J_{P-H} = 1.6 Hz, 15H, $C_5(CH_3)_5$ C), −1.08 (d, J_{P-H} = 10.0 Hz, 9H, $P(CH_3)_3$ B), −1.13 (d, J_{P-H} = 10.4 Hz, 9H, $P(CH_3)_3$ A), −1.33 (d, J_{P-H} = 12.0 Hz, 9H, $P(CH_3)_3$ C), −2.29 (m, 6H, CH_3 A and B), −2.62 (d, J_{P-H} = 6.4 Hz, 3H, CH_3 C). ^{31}P{^{1}H} NMR (D_2O): δ −39.6 (s, $P(CH_3)_3$ B), −40.2 (s, $P(CH_3)_3$ A), −40.5 (s, $P(CH_3)_3$ C). ^{19}F NMR (D_2O): δ −78.1 (s, OSO_2CF_3). TOF MS ES(−) (H_2O/MeOH, 50:50), ◆ = $[Ga_4L_6]^{12-}$, calcd (found), *m*/*z*: 1131.803 (1131.771) [◆ + 4Na$^+$ + 2H$^+$ + 2D$^+$ + **2**]$^{3-}$, 1139.130 (1139.095) [◆ + 5Na$^+$ + 1H$^+$ + 2D$^+$ + **2**]$^{3-}$, 1146.458 (1146.429) [◆ + 6Na$^+$ + 2D$^+$ + **2**]$^{3-}$.

Na$_{11}$[4 ⊂ Ga$_4$L$_6$]. In the glovebox, an NMR tube was charged with **4** (~3 mg, 5 × 10^{-3} mmol) as a solid. This was dissolved in 0.5 mL of D_2O to give a pale yellow solution. A stoichiometric amount of $Na_{12}[Ga_4L_6]$ (~18 mg, 5 × 10^{-3} mmol) was added as a solid to form a bright yellow solution. The NMR tube was then removed from the glovebox and flame-sealed under a static vacuum on a high vacuum Schlenk line. Two diasteomeric host−guest complexes A and B were observed with a dr of 70:30. ^{1}H NMR (D_2O): δ 8.40 (d, J = 7.3 Hz, *aryl*), 8.35 (d, J = 8.3 Hz, *aryl*), 8.17 (d, J = 7.3 Hz, *aryl*), 8.06 (d, J = 7.3 Hz, *aryl*), 8.02 (d, J = 7.3 Hz, *aryl*), 7.92 (d, J = 7.3 Hz, *aryl*), 7.73 (d, J = 7.3 Hz, *aryl*), 7.56 (m, *aryl*), 7.51 (d, J = 7.3 Hz, *aryl*), 7.47 (d, J = 8.3 Hz, *aryl*), 7.46 (br s, *aryl*), 7.19 (d, J = 8.3 Hz, *aryl*), 7.00 (m, *aryl*), 6.85 (d, J = 7.3 Hz, *aryl*), 6.75 (d, J = 7.3 Hz, *aryl*), 6.64 (d, J = 7.3 Hz, *aryl*), 3.61 (m, 2H, *alkenyl* C*H* B), 3.41 (m, 2H, *alkenyl* C*H* A), −0.45 (s, 15H, $C_5(CH_3)_5$ B), −0.54 (s, 15H, $C_5(CH_3)_5$ A), −0.84 (m, 6H, *alkenyl* CH_3 A), −0.92 (m, 6H, *alkenyl* CH_3 B), −1.00 (d, J_{P-H} = 10.1 Hz, 9H, $P(CH_3)_3$ A), −1.23 (d, J_{P-H} = 10.1

Hz, 9H, P(CH_3)$_3$ B), −2.31 (d, J_{P-H} = 6.1 Hz, 3H, CH_3 A), −2.63 (d, J_{P-H} = 6.1 Hz, 3H, CH_3 B). ^{31}P{^{1}H} NMR (D_2O): δ −38.3 (s, P(CH$_3$)$_3$ B), −41.6 (s, P(CH$_3$)$_3$ A). ^{19}F NMR (D_2O): δ −78.1 (s, OSO$_2$CF_3). TOF MS ES(−) (H_2O/MeOH, 50:50), ◆ = [Ga$_4$L$_6$]$^{12-}$, calcd (found), *m*/*z*: 1142.124 (1142.073) [◆ + 5Na$^+$ + 3H$^+$ + **3**]$^{3-}$.

General Procedure for Reaction of Iridium Complexes with Organic Substrates. A thin-wall NMR tube in the glovebox was charged with either **3** or **4** as solids (∼3 mg, 5 × 10^{-3} mmol). This mixture was dissolved in 0.5 mL of D_2O. Dioxane (2 μL) was added via syringe for use as an internal standard. For reactions with host−guest assemblies, Na$_{12}$[Ga$_4$L$_6$] was also added as a solid (∼18 mg, 5 × 10^{-3} mmol). For liquid substrates, excess volume (10 equiv, 10 × 10^{-3} mmol) was added via syringe. For gas-phase substrates, a J. Young NMR tube was used, placed through three freeze−pump−thaw cycles on a vacuum line, and backfilled with 1 atm of the substrate. The solution was shaken briefly. The reaction progress was monitored by NMR spectroscopy at the appropriate temperature. Yields were determined by ^{1}H NMR, as an indeterminate amount of solvent remains on the isolated solid material. Following this general procedure, [**4** ⊂ Ga$_4$L$_6$] reacted with aldehyde substrates to produce encapsulated iridium carbonyl products after 30 min at rt. These products have been previously characterized.[23]

Addition of Cyclopropanecarboxaldehyde to [4 ⊂ Ga$_4$L$_6$]. The reaction was performed by employing the general procedure described above. This solution was let sit at room temperature for 1 h. NMR spectra indicated a mixture of two product diastereomers A and B with a dr of 55:45 in quantitative yield, which were isolated upon removal of solvent in vacuo. Independent formation and encapsulation of Cp*(PMe$_3$)Ir(cyclopropyl)(CO)$^+$ generated identical NMR resonances. ^{1}H NMR (D_2O): δ 8.58 (d, J = 7.2 Hz, *aryl*), 8.49 (d, J = 8.0 Hz, *aryl*), 8.41 (m, *aryl*), 8.26 (m, *aryl*), 8.18 (d, J = 7.6 Hz, *aryl*), 7.92 (m, *aryl*), 7.79 (m, *aryl*), 7.71 (m, *aryl*), 7.58 (m, *aryl*), 7.39 (br m, *aryl*), 7.32 (m, *aryl*), 7.19 (d, J = 8.4 Hz, *aryl*), 7.04 (m, *aryl*), 6.95 (m, *aryl*), 6.89 (m, *aryl*), 6.75 (m, *aryl*), 6.64 (m, *aryl*), −0.04 (br s, 30H, C$_5$(CH_3)$_5$ A and B), −0.57 (m, 18H, P(CH_3)$_3$ A and B), −1.67 (br, *cyclopropyl CH*), −1.79 (br, *cyclopropyl CH*), −2.16 (br, *cyclopropyl CH*), −2.72 (br, *cyclopropyl CH*), −3.14 (br, *cyclopropyl CH*), −3.57 (br, *cyclopropyl CH*). ^{31}P{^{1}H} NMR (D_2O): δ −44.3 (s, P(CH$_3$)$_3$ B), −46.7 (s, P(CH$_3$)$_3$ A). ^{19}F NMR (D_2O): δ −78.1 (s, OSO$_2$CF_3). IR (KBr): 2961, 2021, 1658, 1583, 1547, 1468, 1427, 1393, 1239, 1200, 1066, 785, 744, 641 cm^{-1}.

Addition of Dimethyl Ether to [4 ⊂ Ga$_4$L$_6$]. This was prepared using the general reaction procedure outlined above. Upon heating to 45 °C for 1 h, quantitative formation of encapsulated product observed as two diastereomers A and B in a 88:12 ratio in quantitative yield. Heating the solution to 75 °C overnight results in a thermodynamic dr of 58:42. Independent formation and encapsulation of Cp*(PMe$_3$)Ir(=C(OMe))(H)$^+$ generated identical NMR resonances. ^{1}H NMR (D_2O): δ 8.41 (br s, *aryl*), 8.09 (br s, *aryl*), 7.77 (br s, *aryl*), 7.38 (m, *aryl*), 7.04 (d, J = 7.2 Hz, *aryl*), 6.76 (d, J = 6.4 Hz, *aryl*), 6.62 (d, J = 7.2 Hz, *aryl*), 0.22 (s, 15H, C$_5$(CH_3)$_5$ B), 0.11 (s, 15H, C$_5$(CH_3)$_5$ A), −0.18 (s, 3H, OCH_3 A), −0.55 (d, J_{P-H} = 10.8 Hz, 9H, P(CH_3)$_3$ A), −0.70 (d, J_{P-H} = 10.8 Hz, 9H, P(CH_3)$_3$ B), −18.75 (br, 1H, Ir−*H* B), −19.04 (d, J_{P-H} = 31.2 Hz, 1H, Ir−*H* A). ^{31}P{^{1}H} NMR (D_2O): δ −41.2 (s, P(CH$_3$)$_3$ A), −47.8 (s, P(CH$_3$)$_3$ B). ^{19}F NMR (D_2O): δ −78.1 (s, OSO$_2$CF_3). TOF MS ES(−) (H_2O/MeOH, 50:50), ◆ = [Ga$_4$L$_6$]$^{12-}$, calcd (found), *m*/*z*: 1142.112 (1142.061) [◆ + 6Na$^+$ + H$^+$ + D$^+$ + 5-Me]$^{3-}$.

Addition of Ethyl Methyl Ether to [4 ⊂ Ga$_4$L$_6$]. This was prepared using the general reaction procedure outlined above. Upon heating to 45 °C for 1 h, quantitative formation of encapsulated product observed as two diastereomers A and B in a 54:46 ratio in 71% yield. Independent formation and encapsulation of Cp*(PMe$_3$)Ir(=C(OEt))(H)$^+$ generated identical NMR resonances. ^{1}H NMR (D_2O): δ 8.17 (br s, *aryl*), 7.97 (br s, *aryl*), 7.62 (br s, *aryl*), 7.39 (d, J = 8.1 Hz, *aryl*), 7.34 (d, J = 8.1 Hz, *aryl*), 7.20 (d, J = 7.3 Hz, *aryl*), 7.03 (d, J = 7.3 Hz, *aryl*), 6.85 (d, J = 7.3 Hz, *aryl*), 6.76 (m, *aryl*), 6.62 (m, *aryl*), 1.32 (br m, 4H, OCH_2CH$_3$ A and B), −0.33 (s, 15H, C$_5$(CH_3)$_5$ A), −0.41 (s, 15H, C$_5$(CH_3)$_5$ B), −0.63 (m, 3H, CH_3 A), −0.72 (m, 3H, CH_3 B), −1.25 (m, 18H, P(CH_3)$_3$ A and B), −2.26 (d, J_{P-H} = 6.6 Hz, 3H, CH_3 A), −2.30 (d, J_{P-H} = 6.6 Hz, 3H, CH_3 B), −20.42 (d, J_{P-H} = 33.2 Hz, 1H, Ir−*H* B), −22.12 (d, J_{P-H} = 34.4 Hz, 1H, Ir−*H* A). ^{31}P{^{1}H} NMR (D_2O): δ −35.8 (s, P(CH$_3$)$_3$ B), −36.6 (s, P(CH$_3$)$_3$ A). ^{19}F NMR (D_2O): δ −78.1 (s, OSO$_2$CF_3).

Addition of Cyclopropane to [4 ⊂ Ga$_4$L$_6$]. This was prepared using the general reaction procedure outlined above. The solution was heated in an oil bath at 45 °C for 1 h. The formation of the encapsulated π-allyl product was observed in 74% yield. Independent formation and encapsulation of Cp*(PMe$_3$)Ir(π-allyl)$^+$ generated identical NMR resonances. ^{1}H NMR (D_2O): δ 8.15 (br s, *aryl*), 7.60 (br s, *aryl*), 7.36 (d, J = 8.0 Hz, *aryl*), 7.17 (d, J = 8.0 Hz, *aryl*), 6.82 (br s, *aryl*), 6.74 (d, J = 7.2 Hz, *aryl*), 6.60 (t, J = 7.6 Hz, *aryl*), 0.93 (m, 1H, *allyl*), 0.11 (m, 1H, *allyl*), −0.33 (m, 1H, *allyl*), −0.23 (s, 15H, C$_5$(CH_3)$_5$), −0.33 (m, 1H, *allyl*), −0.67 (m, 1H, *allyl*), −1.25 (d, J_{P-H} = 10.0 Hz, 9H, P(CH_3)$_3$), −1.24 (m, 1H, *allyl*). ^{31}P{^{1}H} NMR (D_2O): δ −46.9 (s, P(CH$_3$)$_3$). ^{19}F NMR (D_2O): δ −78.1 (s, OSO$_2$CF_3). ESI-MS(−) (CD_3OD), ◆ = [Ga$_4$L$_6$]$^{12-}$, *m*/*z*: 1155 [◆ + 8Na$^+$ + **6**]$^{3-}$, 1148 [◆ + 7Na$^+$ + H$^+$ + **6**]$^{3-}$, 1141 [◆ + 6Na$^+$ + 2H$^+$ + **6**]$^{3-}$, 1133 [◆ + 5Na$^+$ + 3H$^+$ + **6**]$^{3-}$, 861 [◆ + 7Na$^+$ + **6**]$^{4-}$, 855 [◆ + 6Na$^+$ + H$^+$ + **6**]$^{4-}$, 850 [◆ + 5Na$^+$ + 2H$^+$ + **6**]$^{4-}$, 844 [◆ + 4Na$^+$ + 3H$^+$ + **6**]$^{4-}$, 839 [◆ + 3Na$^+$ + 4H$^+$ + **6**]$^{4-}$, 684 [◆ + 6Na$^+$ + **6**]$^{5-}$, 680 [◆ + 5Na$^+$ + H$^+$ + **6**]$^{5-}$, 675 [◆ + 4Na$^+$ + 2H$^+$ + **6**]$^{5-}$, 671 [◆ + 3Na$^+$ + **3**H$^+$ + **6**]$^{5-}$.

Addition of H_2 to Na$_{11}$[4 ⊂ Ga$_4$L$_6$]. This was prepared using the general reaction procedure outlined above. The solution was heated in an oil bath at 45 °C for 1 h. The formation of the encapsulated [Ir](D$_3$)$^+$ product was observed in quantitative yield. The newly formed hydride ligands are rapidly exchanged with deuterium from the D_2O solvent and could be observed by ^{2}H NMR spectroscopy. Suitable mass spectra could not be obtained. Independent formation and encapsulation of Cp*(PMe$_3$)Ir(H$_3$)$^+$ generated identical NMR resonances. ^{1}H NMR (D_2O): δ 8.11 (br, 12H, *aryl*), 7.73 (d, J = 7.6 Hz, 12H, *aryl*), 7.37 (d, J = 8 Hz, 12H, *aryl*), 6.99 (t, J = 8 Hz, 12H, *aryl*), 6.80 (d, J = 8 Hz, 12 H, *aryl*), 6.65 (t, J = 8 Hz, 12H, *aryl*), 0.13 (d, J = 1.6 Hz, 15H, C$_5$(CH_3)$_5$), 0.57 (d, J = 11.2 Hz, 9H, P(CH_3)$_3$). ^{2}H{^{1}H} NMR (D_2O): δ −16.9 (br, 3D, D_3). ^{31}P{^{1}H} NMR (D_2O): δ −40.4 (P(CH$_3$)$_3$). ^{19}F NMR (D_2O): δ −78.1 (s, OSO$_2$CF_3).

General Procedure for Determination of Thermodynamic Guest Binding Constants. In the box, an NMR tube was charged with the guest species as a solid (∼3 mg, 5 × 10^{-3} mmol). This was dissolved in 0.5 mL of D_2O. A stoichiometric amount of Na$_{12}$[Ga$_4$L$_6$] was then added (∼18 mg, 5 × 10^{-3} mmol). The NMR tube was capped with a septum and brought out of the box. The total concentration of encapsulated guest was determined using ^{1}H NMR spectroscopy. Alternatively, a stoichiometric amount of a stock solution of the appropriate NR$_4^+$ salt with known binding affinity[19] in D_2O was added via syringe (NEt$_4$OTf or (NPr$_4$)$_2$SO$_4$). The guest replacement reaction was monitored periodically by ^{1}H NMR while heating until no further change in the ratio of guests was observed. The binding constant for the iridium guest can then be calculated from the ratio of encapsulated guests by using the known binding constants for the appropriate ammonium cation.[19] Error analyses for the van't Hoff studies were performed on the slope and intercept of the linear fit.

General Procedure for Kinetics Runs. In the glovebox, stock solutions of Na$_{11}$[**4** ⊂ Ga$_4$L$_6$], TPPTS, PTA, and various salts were prepared using D_2O buffered with either 100 mM KD$_2$PO$_4$/NaOD or 100 mM TRIS/DOTf at pD = 8.0 at room temperature. The pD of the solution was not corrected at different temperatures. An NMR tube capped with a septum was charged with a solution of Na$_{11}$[**4** ⊂ Ga$_4$L$_6$] via syringe such that, upon dilution to 500 μL, a total concentration of 10 mM of the host−guest assembly would be obtained. Appropriate volumes of salt and excess buffer stock solutions were then added to

the NMR tube via syringe. Dioxane (2 μL) was added as an internal standard. The appropriate phosphine solution was then added so that the total solution volume would be 500 μL. The reaction was monitored immediately by ^{1}H NMR at a temperature of 24 °C. The decay of [**4** $\subset$ Ga_4L_6] was monitored using 8 scans with a delay time of 4 s and a 90° pulse of 13.5 μs for each time point. Time points were taken approximately every 5−10 min until the reaction progressed through at least 3 half-lives. The kinetic data were plotted as the concentration of starting material vs time and the exponential decay was fit using KaleidaGraph.[90] The Cp* and PMe_3 resonances for each host−guest diastereomer A and B were used to independently determine k_{obsd} with good agreement. Error analyses for the Eyring plots were performed on the slope and intercept of the linear fit.

Acknowledgment. The authors would like to thank Dorothea Fiedler, Dr. Anna V. Davis, and Dr. Gojko Lalic for helpful discussions. We also thank Dr. Herman van Halbeek for NMR assistance. We thank Dr. Ulla Andersen and Dr. Georg Seeber for obtaining MS data, and the Waters Corp. for use of the TOF spectrometer. This work was supported by the Director, Office of Energy Research, Office of Basic Energy Sciences, Chemical Sciences Division, of the U.S. Department of Energy under Contract DE-AC02-05CH11231.

(90) *KaleidaGraph*, 3.6 ed.; Syngergy Software, 2003.

Supporting Information Available: Tables containing the thermodynamic and kinetic data illustrated in Figures 3, 4, 5, 6, 7, 8, 10, and 11; ^{1}H NMR NOESY of **10** and [NEt_4 $\subset$ Ga_4L_6]; ^{31}P−^{13}C HSMBC of **9**; ^{1}H NMR spectra of host−guest assemblies. This material is available free of charge via the Internet at http://pubs.acs.org.

JA061412W